Babeş-Bolyai University Cluj-Napoca

Faculty of Environmental Science and Engineering

Revisiting optically stimulated luminescence chronologies on loess-paleosol master sections from Europe and beyond

- Doctoral Thesis Summary-

ȘTEFANA-MĂDĂLINA GROZA (SĂCACIU)

Promoters: Prof. Dr. Alida Gabor

Cluj-Napoca 2020

The research discussed in the present thesis was mainly carried out at the Environmental Radioactivity and Nuclear Dating Centre, Interdisciplinary Research Institute on Bio-Nano-Science, Babeş-Bolyai University in Cluj-Napoca, Romania.

Ștefana-Mădălina Groza (Săcaciu) performed one research stages (three months in total) at the Nordic Laboratory for Luminescence Dating (Denmark) and part of the work presented in the current thesis was carried out during this stage.

Ștefana-Mădălina Groza (Săcaciu) benefited from financial support from:

- The Romanian National Authority for Scientific Research CNCS-UEFISCDI through project PN-II-RU-TE-2014-4-1772.
- The Romanian National Authority for Scientific Research, PN-III-P3-3.6-H2020-2016-0015 contract number 7/2016.
- European Research Council (ERC) under the European Union's Horizon 2020 research and innovation program ERC-2015-StG (grant agreement No [678106]).
- EEA-RO-NO-2018-0126 contract nr. 3/2019 "Cave deposits as archives of climate and environmental changes. A Center of Excellence in speleological research".

CONTENTS

3. OPTICALLY STIMULATED LUMINESCENCE INVESTIGATIONS OF LOESS-PALEOSOL SITES FOR THEIR PALEOENVIRONMENTAL IMPORTANCE

Keywords: luminescence dating; optically stimulated luminescence (OSL); fine quartz; coarse quartz; magnetic susceptibility; loess-paleosol master sections; paleoenvironmental and archeological importance of loess; Pleistocene/Holocene transition.

INTRODUCTION

• Optically stimulated luminescence research on loess-paleosol sequences in a paleoenvironmental and archeological context

Recent advances in luminescence dating techniques succeeded in revolutionizing Quaternary science, allowing various sediments and artefacts to be dated like never before. While the application of thermoluminescence (TL) continues, the current developments are mainly associated with optically stimulated luminescence (OSL). Since Huntley et al. (1985) introduced the principle of OSL dating 35 years ago, a firm connection with loess research has developed in order to decipher Quaternary events. Spanning the last ~2.6 Ma, the Quaternary includes the Pleistocene and the Holocene epochs and is known not only for climate changes and their effects on the environment, but also for the evolution of humans.

Optically stimulated luminescence dating is considered to be an ideal technique for eolian environments such as loess-paleosol deposits. The minerals used commonly in OSL are quartz and feldspar, which are the most abundant in the Earth's continental crust and which act as natural dosimeters, storing energy while being subjected to natural radiation. A common approach in optical dating is to employ the single aliquot regenerative-dose (SAR) measurement protocol (Murray and Wintle 2000, 2003). Nevertheless, several issues have been raised when using the SAR protocol on quartz grains.

Recent studies reported age underestimations for samples which are older than 70 ka (e.g. Murray et al., 2007; Buylaert et al., 2007; Timar et al., 2010). Furthermore, ages obtained on fine (4-11 μm) and coarse (63-90 μm) quartz from Romanian sites appeared to underestimate true burial ages, with the fine quartz displaying an earlier and more severe underestimation (e.g. Timar-Gabor et al., 2011; Constantin et al., 2015). It is also important to mention the fact that at a global scale, for samples older than 40 ka (Timar-Gabor et al., 2017) and even younger than 30 ka (Groza-Săcaciu et al., 2020), different results were reported for equivalent doses between the two quartz fractions, with systematically higher values being obtained for the coarse (63-90 μm) grains. Moreover, while investigating the saturation characteristics for the fine (4-11 μm) and coarse (63-90 μm) quartz grains (Constantin et al., 2012; Timar-Gabor et al., 2012, 2015b), it was observed that the dose response curves for the two fractions diverge at doses higher than ~100 Gy, with fine (4-11 μm) quartz displaying higher saturation characteristics. Last but not least, a final discrepancy was observed between the natural and the laboratory dose response curves for the two quartz fractions (Timar-Gabor and Wintle, 2013; Timar-Gabor et al., 2015b; Constantin et al., 2015). So

far, all these experimental observations have not been comprehensively explained. It is clear that relying on only one quartz fraction in order to obtain accurate OSL chronologies is not sufficient, especially since it is essential that reliable high-resolution age results are obtained in other to fully assess Quaternary events.

The current thesis presents several results which pertain to the research project INTERTRAP- Integrated dating approach for terrestrial records of past climate using trapped charge methods (StG 678106, HORIZON 2020) which was financed by the European Research Council (ERC). The contribution of the current thesis refers to additional investigations on the perplexing OSL results reported on loess-paleosol sites from Europe and China and the assessment of the environmental response to the Pleistocene/Holocene transition recorded at loess-paleosol sites. An added value to the INTERTRAP project was brought by the OSL investigation at two Austrian archeological sites (Krems-Wachtberg and Kammern-Grubgraben).

- **Outline of the dissertation**

The doctoral dissertation comprises 4 main chapters. **Chapter 1** presents an overview of loess deposits worldwide and their importance as terrestrial archives of the Quaternary, with several loess-paleosol master sections from the Eurasian loess belt being presented. **Chapter 2** introduces the basic concepts of optically stimulated luminescence dating and focuses on the application of the SAR protocol (Wintle and Murray 2000, 2003) on quartz. **Chapter 3** reports result from OSL investigations on three loess-paleosol sites of paleoenvironmental importance in 3 subchapters. The first subchapter presents a new OSL chronology from Mircea Vodă loess-paleosol master section and additional investigations regarding the saturation characteristics of dose response curves constructed up to high doses for quartz grains (**Groza-Săcaciu et al., 2020**). The second subchapter assesses the Pleistocene/Holocene transition as recorded at the Râmnicu Sărat and Mircea Vodă (Romania) loess-paleosol sites based on SAR-OSL and magnetic susceptibility data, with the results being compared to two other regional sites - Roxolany (Ukraine) and Mošorin (Serbia) and the marine and ice core records (Constantin et al., 2019). The third subchapter presents preliminary results from the Chinese loess section of Luochuan which will be part of future publications. **Chapter 4** reports result from OSL investigations on two Austrian loess-paleosol sites which preserved important archeological findings – Krems-Wachtberg (**Subchapter 4.1**; Groza et al., 2019) and Kammern-Grubgraben (**Subchapter 4.2**; Händel et al., 2020).

1. THE IMPORTANCE OF LOESS-PALEOSOL SEQUENCE

1.1. Loess - an overview

1.1.1. Definition of loess

In the past decade, an increasing interest has been shown in the interdisciplinary study of mineral dust, as it has been determined that dust has a significant impact on global radiation and carbon balance and can also be regarded as an indicator of paleoclimatic changes by way of geologic records (Muhs, 2013). While the term 'dust' refers to the solid particles found in suspension in a gaseous setting (Pye, 1987), the particular type that accumulates as terrestrial sediments is known as loess. There have been numerous attempts to define the term 'loess' (Roberts, 2008 and references therein), the simplified version being that of a terrestrial sediment dominated by silt, formed by dust which was entrained, carried and deposited by wind (Pye 1987, 1995; Muhs, 2007).

1.1.2. Origin of loess deposits

While defining loess is still a subject of discussion, the origin of loess deposits is considered even more controversial, with most debates focusing on the processes behind the formation of silt particles. At the moment, the two proposed versions are the "glacial loess model" and "desert loess model" (Li et al. 2020 and references therein). Other sources for silt-sized particles like sedimentary rocks (especially shales and siltstones) or volcanic ash (mainly in Iceland, Alaska, South America, and New Zealand) are often neglected. It is very probable though that loess deposits are a result of both non-glacial and glacial processes (Muhs et al., 2014).

1.1.3. Mineralogy and geochemistry

The mineralogy and geochemistry of loess deposits is influenced by the geology of the source areas (Muhs and Bettis, 2003). Clay-sized grains are usually phyllosilicates such as smectite, mica, vermiculite, kaolinite, and chlorite. Coarse (> 4 μm) grains, however, represent primary rock-forming minerals originated from igneous rock formation such as quartz, K-feldspar, plagioclase, calcite, and dolomite (Muhs, 2013). Heavy minerals are typically present but only in small amounts. From a geochemical point of view, SiO_2 is generally found in loess deposits between 55 and 65%, indicating the dominance of quartz. The remainder is represented by feldspars (5-30%), mica (5-10%), carbonates (0-30%) and clay materials (10-15%) (Pye, 1987).

1.1.4. Sedimentology and stratigraphy

The grains within the loess sediments can have a wide range of sizes, being transported through short-term and long-term suspension and through saltation (Pye, 1987). The modal grain size is usually that of 30 μm, with sand (63 μm -2 mm) and clay (< ~4 μm) in lower quantities and silt-sized (~4-63 μm) particles in higher quantities (Pye, 1995; Roberts, 2008). Dust particles can settle through dry deposition, wet deposition and vegetation (Pye, 1995).

In loess, primary structures are subtle and generally lacking. Second structures caused by fauna and flora lead to material mixing and disturbance of geological units called bioturbation. Loess sections usually comprise of alternating soil horizons, loess sedimentation and pedogenesis, which should be regarded as competing processes (Verosub et al, 1993). Regarding the soil horizons, most researchers advocate for the "top-down" soil genesis model. Nevertheless, this model has been proven to be inapplicable to elevated landscapes, where dust accumulation is more frequent. This leads to upward growth of the soil profile, also described as cumulization (Jacobs and Mason, 2007; Schaetzl and Anderson, 2005).

1.1.5. Distribution of loess deposits worldwide

Loess is known to cover around 10% of the continental surfaces of both northern and southern hemispheres (Pye, 1987). In Eurasia, loess sites are distributed at a latitude between 30 and 60° N (Muhs, 2007). In Europe, loess is found scattered from France to Russia, adjacent to major river systems. In Asia, significant loess deposits are found in Siberia, Central Asia, and China. China stands out as the country with the most extensive and continuous loess area (the Central Loess Plateau).

In North America loess can be found as extensive deposits in the Palouse area, Snake River Plain, the Great Plains region and the Mississippi Valley basin, with discontinuous deposits being present in Alaska and the Yukon Territory (Canada) (Péwé, 1975; Bettis et al., 2003; Busacca et al., 2004). In regard to South America, loess is mostly found in the Gran Chaco region (northern Argentina, Paraguay, and Bolivia) and in the Pampas of central Argentina (Zárate, 2003). Africa and the Middle East lack in extensive loess deposits., with limited loess and loess-like areas being found in Namibia, Nigeria, Libya, Tunisia, Canary Islands, Cape Verde Islands, and Israel. New Zealand is also known to have extensive loess accumulations which have been intensely studied (e.g. Berryman, 1993; Eden and Hammond, 2003).

1.2. Loess-paleosol sequences as terrestrial archives of the Quaternary

1.2.1. Paleoenvironmental importance

Loess-paleosol sequences are regarded as analogs to marine and ice records and powerful tools in acquiring paleoenvironmental information regarding the Quaternary. The major climatic changes have been proven to display a periodicity influenced by the Milankovitch cycles, more precisely by the orbital forcing through precession (19 ka, 23 ka), obliquity (41 ka) and eccentricity (100 ka) (Milankovitch, 1949). The 100-ka cycle is believed to have led to cold climates with extended glacier development (glacials) and warmer climates (interglacials). More rapid climate oscillations are also known to have taken place in the last 80 ka and are associated to cooler events (stadials) and warmer events (interstadials). In the Northern Hemisphere, such examples of abrupt climatic shifts are the Dansgaard-Oeschger (D-O) cycles and Heinrich events.

Understanding the reasons behind these past climate variations could play a key role in predicting the changes that await us in the future. In that regard, loess-paleosol sequences are able to provide paleoclimate data through multiple scientific methods, with loess yielding information about the glacial periods and paleosols about interglacial and interstadial periods. The most popular investigative method since the 1980s has been the measurement of mineral magnetic properties, especially the magnetic susceptibility (MS) (e.g. Kukla and An, 1989; Verosub et al., 1993). For Europe, China and North America, this technique allows for section-to-section correlation since numerous studies in these regions have shown high magnetic susceptibility in paleosols and low magnetic susceptibility in loess (Kukla et al, 1988; Kukla and An, 1989). Another advantage of this technique is the possibility to correlate MS with other proxies as dust records in ice from Greenland and Antarctica and deep-sea oxygen isotope records (Heller and Liu, 1984). The paleomagnetic reversals of the geomagnetic field also yield a chronostratigraphic framework.

Biological (e.g. lipids from bacteria and plant waxes) and geochemical (e.g. elemental and stable isotope ratios, soil color, granulometric analysis) proxies can also be used in order to provide information regarding paleoenvironmental changes from loess-paleosol deposits. Geochronological control can be achieved through radiocarbon dating and amino acid racemisation when fossils exist. Direct dating of loess-paleosol sequences is possible through luminescence methods (thermo-luminescence and optically stimulated luminescence) and electron spin resonance (ESR) method.

1.2.2. Archeological importance

Besides being considered a period of perpetual climatic shifts, the Quaternary is also regarded as the "Age of Humans". It was during the Early Pleistocene that the genus *Homo* appeared in Africa, later dispersing around the globe, and evolving into the Anatomically Modern Human (AMH). With thicker loess deposits generally located in the proximity of river systems with fertile plains, prehistoric human settlements have been found preserved in these eolian deposits, mostly in Europe and Asia. In central and eastern Europe, for example, the high rates of loess deposition during the Middle Pleistocene lead to the conservation of numerous archeological sites (Dodonov et al., 2006). In China, loess deposits are strongly linked to the origin and development of Chinese culture (Smalley, 1968; Dong et al., 2012).

The fact that loess represents a low-energy sedimentary environment and possesses generally alkaline conditions helps preserve artifacts and bone remains (Zárate, 2016; Händel et al., 2009). In addition to this, the homogeneous aspect of loess result in a higher visibility of archeological remains compared to different non-eolian sedimentary settings (Zárate, 2016). Coupled with the paleoenvironmental information supplied by loess-paleosol sequences, researches are able to reconstruct the prehistoric ways of life and to work out long-lasting debates, such as the arrival in Europe of the earliest modern *Homo* (Conrad and Bolus, 2003; Mellars, 2011; Iovita et al., 2014).

1.2.3. Loess-paleosol master sections

From all the loess deposits that exist around the world, the Eurasian loess belt in particular is the most important Quaternary terrestrial archive, providing some of the most intensely studied LPSs. These sequences are regarded as master sections, outstanding through their paleoenvironmental and archeological significance.

For the Chinesse Loess Plateau, the most comprehensive and researched loess deposit is Luochuan, which represents a 2.5 Ma long record of climatic changes expressed through more than 30 loess-paleosol alternations. It is for this site that Heller and Liu (1984) and Kukla and An (1989) observed the variations of magnetic susceptibility in loess and paleosol units and the correlation of the magnetic record with the marine oxygen isotope record. Here, multi-proxy analysis (e.g. Zhisheng et al., 1989; Zhang et al., 2008; Nugteren et al., 2004; Yang et al., 2001) alongside radiocarbon (T.S. Liu, 1985) and luminescence dating (e.g. Y.C. Lu et al., 2007) offered valuable information regarding the paleoclimatic and paleoenvironmental changes controlled by the East Asian Monsoon and Milankovitch cycles and additionally

linking the section, from a geochemical point of view, with other LPSs from Europe and Argentina.

In Europe, the middle and lower Danube basins feature the most significant pre-Late Pleistocene LPSs (Bronger, 2003; Buggle et al., 2009). Numerous studies have been particularly focusing on the deposits located in the Vojvodina region, in northern Serbia. Titel is such a loess deposit where extended studies were undertaken (e.g. Bokhorst et al., 2009; Bokhorst and Vandenberghe, 2009; Marković et al., 2008). In Romania, Mircea Vodă is regarded as a master section due to its 26 m thick alternation of 6 well developed pedocomplexes, being researched since the 70's (e.g. Conea, 1969, 1970; Buggle et al., 2008; Panaiotu et al, 2001; Timar-Gabor et al., 2011).

Roxolany (Ukraine) is the most important loess-paleosol sequence in the Black Sea area considered to play an important part in the correlation of European and Chinese loess deposits on a regional and interregional scale, yielding important paleoclimatic and paleoenvironmental information during the whole Pleistocene (Nawrocki et al., 2018). Also located in Ukraine, the Stayky section is another important LPS, where the upper part of the sequence recorded rapid climatic shifts similar to the Nussloch LPS from Germany.

The Nussloch master section has both a paleoenvironmental and a geo-archeological importance, exhibiting a thick and detailed stratigraphy of the Late Pleistocene and preserving a unique Upper Paleolithic cultural level attributed to AMH (Kind, 2000). Last but not least, probably the most important archeological discovery has been at Krems-Wachtberg, Austria, where numerous studies lead to linking the high-resolution record of climatic conditions with the presence of the AMH north of the Alps (e.g. Einwögerer et al., 2014; Händel et al., 2008; Zeeden et al., 2015; Lomax et al., 2014).

2. BASIC CONCEPTS OF OPTICALLY STIMULATED LUMINESCENCE DATING

2.1. General principles

The luminescence phenomena refer to electromagnetic radiation (normally in the form of visible light) emitted by materials as a result of an external stimulation such as heat, ionizing or electromagnetic radiation, pressure, or chemical reaction. In the past few decades, the analytical dating methods pertaining to luminescence are thermoluminescence (TL) and optically stimulated luminescence (OSL), depending on the type of stimulation – heat or light, respectively.

The moment which is dated represents the last resetting of the luminescence 'clock' to zero. In the case of sediments, the signal resetting is caused by sunlight exposure of grains during erosion and transportation. After deposition, the mineral grains will be covered allowing the luminescence signal to build up again. Under controlled laboratory conditions, by stimulating the grains with heat or light the signal can be quantified for determining the time passed since the last zeroing event.

2.2. Luminescence mechanisms

In general, for luminescent materials (insulators and semi-conductors), the mechanism is described on account of a solid-state physics model explaining energy transfer processes of electrons. According to the energy level model in a crystalline lattice, a valence band and a conduction band are separated by a 'forbidden energy gap' (band gap). Since natural minerals have an imperfect crystal structure, defects will give rise to the creation of allowed temporary energy states within the band gap. When ionizing radiation interacts with the crystal lattice, electrons from the valence band may gain sufficient energy to make the transition to the conduction band. For every electron which is promoted, a hole (positive charge) is created in the valence band. The unstable and excited electrons lose the excitation energy and return in the valance band or get trapped at a defect within the band gap. The same process is applicable to holes. By exposing the crystal to thermal or optical stimulation, electrons may absorb sufficient energy in order to return to the conduction band, after which they may become trapped again or recombine with holes in recombination centers, releasing energy as it does so. When the electron-hole recombination results in energy release in the form of photon emission, the process is called luminescence. The foregoing description applies for the general one trap (GOT) model.

2.3. Laboratory measurements for obtaining the age

When dating sediments, the resulting age will reflect the moment of deposition. Ideally, the signal would have been completely removed by exposure to sunlight, in which case the basic equation used is:

$$Age = \frac{Equivalent\ dose}{Annual\ dose}$$

where the equivalent dose (Gy) is a combined received dose from exposure to α, β and γ radiation, and the annual dose (Gy a^{-1}) is the radiation energy absorbed annually per unit of mass.

2.3.1. Obtaining the equivalent dose

As previously stated, measuring the trapped electron population in the laboratory is based on a mechanism similar to the zeroing event (heat or light). The mineral grains are stimulated with an amount of energy sufficient to de-trap the electrons, obtaining a signal (from electrons-luminescence centers recombination) in the form of an OSL decay curve (luminescence intensity as a function of time). The natural luminescence signal is further used in order to establish the total absorbed dose during burial (equivalent dose, ED). This is done by calibration with an OSL signal obtained through known laboratory radiation doses in the form of a dose response curve. The way of determining the equivalent dose can vary depending on the measurement procedures and the type of mineral investigated.

2.3.2. Obtaining the dose rate

The annual dose reflects the rate at which the mineral grains from the sediment absorbed the radiation energy from the environment. The dose is divided into an internal dose (from α and β radiation emitted from within the mineral grains) and external dose (α, β and γ radiation from the ambient matrix and cosmic radiation). The ionizing radiation is provided by the naturally occurring long-lived radionuclides ^{238}U, ^{235}U, ^{232}Th and their daughters ^{87}Rb and ^{40}K. Various methods can be used and these can be either indirect such as neutron activation analysis (NAA), inductively coupled plasma-mass spectrometry (ICP-MS), atomic absorption spectrometry (AAS), and gamma-ray spectrometry, or direct such as alpha or beta counting. The type and size of mineral grains, water content, latitude, depth, and altitude must be taken into consideration, with conversion factors being employed in deriving the annual dose (e.g. factors tabulated by Adamiec and Aitken, 1998 or Guérin et al., 2011).

2.4. Luminescence minerals used for sediment dating – case study on quartz

Dating sediments has been so far limited to quartz and feldspar. These natural dosimeters are preferred not only due to their abundance in different sedimentary environments and their resistance to weathering, but also due to their stable luminescence signal over geological timescales which can be sufficiently reset (bleached) by exposure to sunlight. Quartz, in particular, is the second most abundant mineral after feldspar in the continental crust. With its simpler crystal structure compared to feldspar, relevant properties for optically stimulated luminescence and advances in applicable protocols, quartz is considered a more reliable material and is often preferred for luminescence applications (**Wintle, 2008**).

2.4.1. Quartz origin and structure

Quartz and other silica minerals make up for 12.6% of the mass of the Earth's continental crust. It occurs in almost all acid igneous, metamorphic and sedimentary rocks. In sedimentary deposits quartz grains originate mainly from recycled sediments, metamorphic rocks and siliceous igneous rocks and rarely hold a volcanic or diagenetic provenance. The origin and formation history of individual quartz grains play a key role in the OSL characteristics of due to various concentrations of point defects created within the crystal lattice (Preusser et al., 2009).

From a chemical point of view, quartz is composed almost 100% from Si and O, the bond between the two elements being of 40% ionic and 60% covalent nature. Quartz exists in two forms – alpha or beta. For alpha quartz, the basic component of the crystal structure is the $[SiO_4]^{4-}$ tetrahedron, linked to the neighboring tetrahedra by oxygen ions and forming angular connected hexagons.

2.4.2. Energy band model for quartz

A pioneer in OSL, Huntley et al. (1985) was the first to suggest that the GOT model cannot adequately explain the luminescence phenomenon. The OSL signal comprises 'fast', 'medium' and 'slow' components (Smith and Rhodes, 1994; Bailey et al., 1997). A complete review of the OSL components is included in Wintle and Adamiec (2017). Bailey (2001) generated an energy band model for quartz accompanied by selected parameters (e.g. trap depth energies) and mathematical treatment. This model displays five electron trapping centers below the conduction band at different depths and four recombination centers close to the valence band.

2.4.3. Sample and aliquot preparation

The procedures for extracting the quartz fractions from the mixed sedimentary sample are performed under low intensity red light conditions in order to avoid bleaching the luminescent signal. After removing the end material from the stainless-steel tubes, the core material is subjected to chemical treatments, sieving, separation in Atterberg cylinders and centrifugations in order to extract different quartz fractions.

2.4.4. The single-aliquot regenerative-dose (SAR) procedure

The SAR procedure was developed particularly for the OSL fast component in quartz (Preusser et al., 2009). **Table 2.1** presents the measurement scheme. The end result will consist of a sensitivity corrected dose response curve derived from the L_x/T_x ratio onto which the natural OSL signal is interpolated in order to obtain the equivalent dose. The SAR protocol has several intrinsic tests so that its performance can be verified for each measured aliquot. The recycling test is used for assessing the efficiency of the sensitivity correction. The reliability of the corrected dose response curve. is done through a recuperation test. The infrared (IR) depletion test (Duller, 2003) detects feldspar contamination. Besides these aliquot validation tests, additional investigations can be performed such as the preheat plateau and dose recovery tests.

Table 2.1. The generalized SAR protocol for quartz (after Murray and Wintle, 2003).

Step	Treatment
1.	Give dose (D_i)[a]
2.	Preheat (160-300 °C for 10 s)
3.	Blue stimulation for x seconds at 125 °C (L_x)[b]
4.	Give test dose (D_t)
5.	Cutheat (T< preheat)
6.	Blue stimulation for x seconds at 125 °C (T_x)
7.	Blue stimulation for 40 s (T> preheat)
8.	Return to step 1

[a] When measuring the natural signal in the first cycle, i = 0 and $D_0 = 0$.

[b] The blue stimulation time is conditioned by the stimulation light intensity.

2.4.5. OSL dating using the SAR protocol on sedimentary quartz – highlights and challenges

The improvements made in luminescence research have led to an increased reliability in quartz as a retrospective dosimeter and in the SAR protocol as a robust dating technique. The SAR procedure presents many advantages such as a higher precision (normally 5-10%) and the ability to detect microdosimetry variations or

partial bleaching. The measurement protocol enables sensitivity change corrections, excellent reproducibility, intrinsic routine tests, and high throughput. Moreover, ages derived from quartz extracts of different ages, originating from a variety of environmental settings and geographic areas were in agreement with chronologies obtained independently (e.g. Murray and Olley, 2002; Constantin et al., 2012; Anechitei-Deacu et al., 2014; Trandafir et al., 2015).

Numerous OSL studies have reported the fact that the luminescence properties of sedimentary quartz are directly affected by grain history, geological origin, trace element geochemistry or sample radiation history (Adamiec, 2000; Duller et al., 2000; Duller, 2004). Poor OSL signals, signal fading, inadequate bleaching, thermal transfer, low saturation dose or cycles of sediment reworking can have a significant impact in obtaining an accurate luminescence age (Preusser et. al., 2009). For eolian sediments such as loess-paleosol sequences, OSL ages may appear erroneous for reasons such as suboptimal pre-depositional bleaching, post-depositional mixing due to pedo- and bioturbation (e.g. Zech et al., 2017) or highly contaminated quartz extracts (Groza et al., 2019).

Dating studies have reported an equivalent dose and age discrepancy between different quartz fractions extracted from European and Chinese loess sections (Timar-Gabor et al., 2017). Another intriguing fact is that alongside the chronological issue, the saturation characteristics for the fine (4-11 μm) and coarse (63-90 μm) quartz are different, with coarse grains saturating sooner despite fine fraction underestimating the true ages before the coarse one (e.g. Timar-Gabor et al., 2017). The relationship between the saturation characteristics and grain diameter was presented by Timar-Gabor et al. (2017). Another issue is the discrepancy between the natural and the laboratory dose response curves for different quartz fractions (Chapot et al. 2012; Timar-Gabor and Wintle 2013). This observation undermines one of the main assumptions of SAR-OSL protocol stating that the laboratory dose response curve reproduces the natural signal growth. As a result, Chapot et al. (2012) suggested an ED of 150 Gy as a maximum limit for OSL dating, while Timar-Gabor and Wintle (2013) and Constantin et al (2015a) recommend caution from ~100 Gy to 200 Gy.

3. OPICALLY STIMULATED LUMINESCENCE INVESTIGATIONS IN LOESS-PALEOSOL SITES FOR THEIR PALEOENVIRONMENTAL IMPORTANCE

3.1. Single aliquot regeneration (SAR) optically stimulated luminescence dating protocols using different grain-sizes of quartz: revisiting the chronology of Mircea Vodă loess-paleosol master section (Romania)

3.1.1. Introduction

It is well known that the results of luminescence dating methods applied on quartz underestimate the expected ages for samples collected below the paleosol associated with Marine Isotope Stage (MIS) 5, as reported at Mircea Vodă loess paleosol site, Romania (Timar et al., 2010), and at various sites in China (Buylaert el al., 2007, 2008). Another key issue which was raised relates to the choice of the quartz grain size and the discrepancies between the age results for values higher than 40 ka. In the light of these findings, the SAR dating protocol on quartz of different grain sizes was applied for revisiting the chronology of Mircea-Vodă loess paleosol sequence.

3.1.2. Location and importance

The loess-paleosol archive from Mircea Vodă (48°19'15" N, 28°11'21" E) is situated in the Dobrogea region, in the proximity of the Danube River, the Black Sea and the Karasu valley. It is regarded a key section, being one of the most studied sections in Eastern Europe. Previous sedimentological, geochemical and environmental magnetic results showed that the loess from Mircea Vodă displays similarities with the loess from Serbia (Vojvodina) and China (Chinese Loess Plateau) (Buggle et al., 2008, 2009, 2014; Necula and Panaiotu, 2012; Necula et al., 2013).

3.1.2.1. Stratigraphy

The Mircea Vodă section displays six pedocomplexes, comprising at least 700 ka of paleoclimate. The S_0 layer is a steppe soil which displays similarities with the L_3 unit in what regards magnetic granulometry (Buggle et al., 2008; Necula and Panaiotu, 2012). An interstadial pedocomplex (L_1S_1) of the last glacial cycle is comprised in the L_1 unit (Timar et al., 2010; Buggle et al., 2008). The S_1 pedocomplex has been identified as a gray-brown fossil steppe soil (Bălescu et al., 2010; Buggle et al., 2009). The S_2 pedocomplex has also been identified as a gray-brown fossil steppe soil (Bălescu et al., 2010; Buggle et al., 2014). The S_3 unit can be identified as a fossil steppe or forest-steppe

soil (Buggle et al., 2014). The S_5 paleosol is correlated with MIS 13-15 and has been classified as a fossil (chromic) Cambisol and Luvisol (Buggle et al., 2013).

3.1.2.2. Previous studies on Mircea Vodă section

Mircea Vodă was the first section in Romania to be dated using optically stimulated luminescence (OSL) methods based on fine quartz (4–11 μm) by Timar et al. (2010). At the same time, Bălescu et al. (2010) investigated alkali feldspars extracted from three samples taken from L_1, L_2 and L_3 loess units. The quartz luminescence study of Timar et al. (2010) focused on the last four glacial periods, with 9 samples being taken from the uppermost loess layer (L_1) and three more from L_2, L_3 and L_4 loess units, respectively. Timar-Gabor et al. (2011) later presented a comparison on ages obtained on coarse (63–90 μm) quartz. The same samples have been investigated by Vasiliniuc et al. (2012, 2013b, 2013a) by using polymineral fine (4–11 μm) fraction extracted from the same material used by Timar et al. (2010).

3.1.2.3. Luminescence characteristics ad behavior

The first OSL chronology obtained for the Mircea Vodă section was reported by Timar et al. (2010) on fine (4–11 μm) quartz fraction extracted from 12 samples (MV 01–13). Later on, Timar-Gabor et al. (2011) focused on the coarse (63–90 μm) quartz fraction obtained from the same samples. The luminescence characteristics were studied by applying the SAR protocol (Murray and Wintle, 2000). LM-OSL dose response curves (DRC) were constructed up to 1 kGy (Timar-Gabor et al., 2012).

However, the equivalent doses obtained on fine (4–11 μm) quartz were lower than those obtained on coarse (63–90 μm) quartz (Timar et al., 2010; Timar-Gabor et al., 2011). Pulse annealing measurements on both quartz fractions have been employed in order to assess the potential contamination of the OSL dosimetric trap with an unstable component. Later on, Timar-Gabor et al. (2012) further investigated dose response curves up to 10 kGy for both quartz grain sizes and Timar-Gabor et al. (2015b) investigated the reproducibility of the dose response curves up to 15 kGy on coarse (63–90 μm) quartz.

The site has also been investigated by Bălescu et al. (2010) on 60–80 μm alkali feldspars grains. Bearing in mind the issues rose by the quartz results, Vasiliniuc et al. (2012, 2013b, 2013a) focused on luminescence properties and ages obtained for polymineral fine (4–11 μm) material extracted from previously investigated samples by Timar et al. (2010).

3.1.3. Current study on Mircea Vodă

3.1.3.1. Sampling, preparation, and analytical facilities

For the current study, investigations were performed on 20 new samples from Mircea Vodă section. The first 12 samples (2MV 40–MV 2.6) were taken from the Pleistocene/Holocene transition, while doublet samples (2MV 570, L3, L4 and L5) were taken directly beneath the S_1–S_4 units, respectively. Standard laboratory sample preparation was then performed under red light conditions. The samples were measured on Risø TL/OSL-DA-20 readers (Thomsen et al., 2008). Radionuclide specific activities were measured though high-resolution gamma spectrometry.

3.1.3.2. Luminescence measurements

For ED determination for the fine (4–11 μm) and coarse (63–90 μm) fractions the single-aliquot regenerative dose (SAR) protocol was used (Murray and Wintle, 2000, 2003). To corroborate the previous quartz studies on Mircea Vodă, the ED dependency on the preheat treatment was assessed for one doublet sample from the L_4 unit concluding that there is no systematic variation for the 200–280 °C temperature range. For determining equivalent doses at least 8 aliquots have been measured per sample per quartz fraction (**Table 3.1.1**).

In order to assess the closeness to saturation of the coarse quartz (63–90 μm) natural signal, CW-OSL growth curves were constructed up to 1 kGy for the old samples taken from L_3, L_4 and L_5 loess units. The natural signal reached between 71% and 87% of the laboratory saturation level. All equivalent doses are presented in **Table 3.1.1**. For both quartz fractions, the average sensitivity-corrected natural signals (L_{nat}/T_{nat}) for the 2MV 570, 2MV L3, 2MV L4 and 2MV L5 samples were plotted as a function of the expected ED. Bearing in mind the fact that these samples were taken directly under the paleosol units, the expected ages were found based on the climatic records of benthic $\delta^{18}O$ (Lisiecki and Raymo, 2005). It can be noted that the samples are in field saturation, meaning that the natural signals are no longer increasing with depth. The ratios of the natural signals to laboratory saturation levels for the two grain sizes are in agreement with previous reports from Timar-Gabor et al. (2012) for an infinitely old sample.

Extended CW-OSL growth curves were subsequently constructed for samples 2MV L3A and 2MV L4A up to 5 kGy (for 4–11 μm quartz grains) and 2 kGy (for 63–90 μm quartz grains) using at least 6 regenerative points and a test dose of 17 Gy as well as a test dose of 170 Gy (**Figure 3.1.1a–d**).

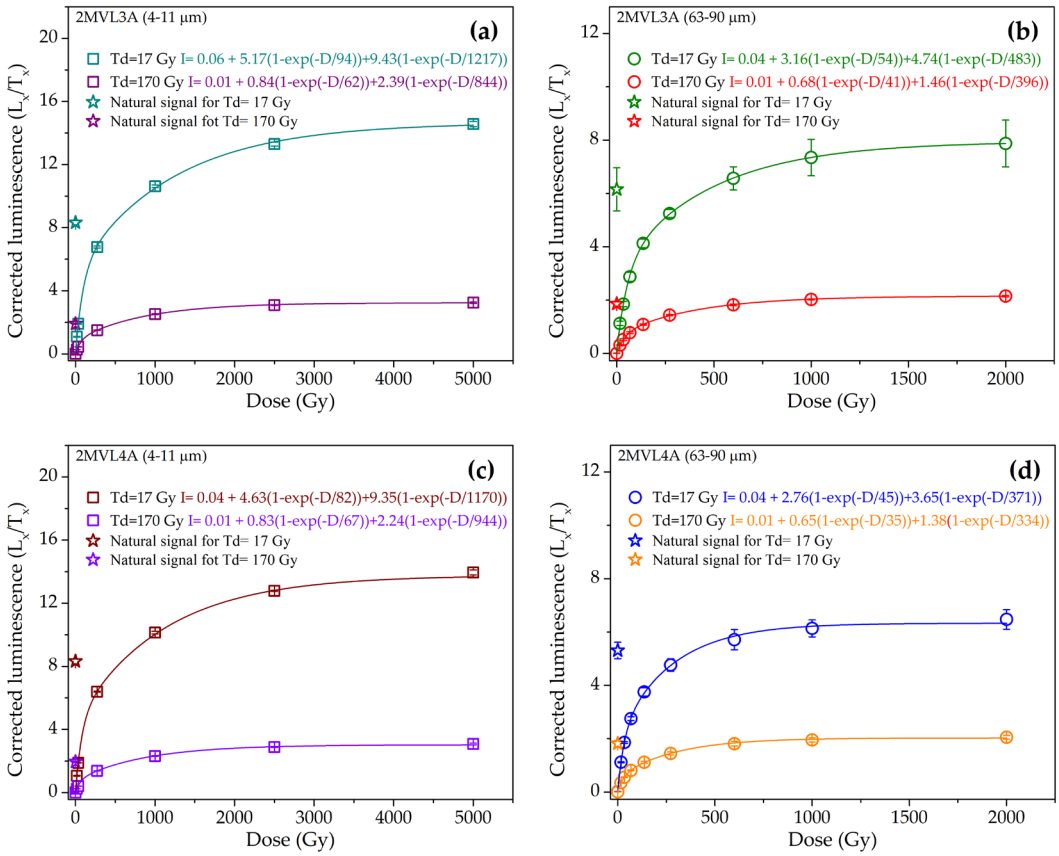

Figure 3.1.1. Comparison of growth curves for samples 2MV L3A (**a**, **b**) and 2MV L4A (**c**, **d**) for both quartz fractions. The curves were best described by a sum of two exponentials function. At least three aliquots have been used in order to obtain the average corrected luminescence signals used to construct the growth curves. A preheat temperature of 220 °C for 10 s and a cutheat of 180 °C have been employed.

Table 3.1.1. Summary of the equivalent doses, radionuclide activities, calculated dose rates and optical ages. The luminescence and dosimetry data are indicated alongside the random uncertainties and the optical ages are indicated alongside the overall uncertainties. All uncertainties are standard uncertainties. Specific activities were measured on a well detector by high resolution gamma spectrometry. The ages were calculated assuming water content of 20%. The total dose rate includes the contribution from cosmic rays (Prescott and Hutton, 1994), gamma, beta, and alpha (for 4–11 µm quartz grains) radiations. An internal dose rate of 0.01 ± 0.002 Gy/ka (Vandenberghe et al., 2008) alongside a beta attenuation and etching factor of 0.94 ± 0.05 (Mejdahl, 1979) were taken into consideration for the coarse (63–90 µm) quartz fraction. The alpha efficiency factor for the 4–11 µm quartz grains was that of 0.04 ± 0.02 (Rees-Jones, 1995). The optical ages marked with asterisk (*) were obtained for samples which were found to be close to saturation levels (between 71% and 87%)

Unit Code	Sampling Depth (m)	Laboratory Code	Grain Size (μm)	Equivalent Dose (Gy)	Recycling Ratio	Recuperation (%)	IR depletion Ratio	Total dose Rate (Gy/ka)	Cosmic dose Rate (Gy/ka)	Age (ka)	Random Error (%)	Systematic Error (%)
S_0/L_1	0.4	2MV 40	4–11	15.4 ± 0.2	1.02 ± 0.01	0.11 ± 0.03	0.99 ± 0.01	2.91 ± 0.05	0.22 ± 0.03	5.3 ± 0.5	2.3	9.9
			63–90	12.9 ± 1.5	1.03 ± 0.01	0.15 ± 0.07	0.98 ± 0.01	3.44 ± 0.05		5.3 ± 0.7	11.8	7.6
S_0/L_1	0.5	2MV 50	4–11	20.3 ± 0.3	1.02 ± 0.01	0.07 ± 0.03	0.95 ± 0.01	3.05 ± 0.07	0.21 ± 0.03	6.7 ± 0.7	2.7	9.9
			63–90	17.3 ± 1.9	1.05 ± 0.01	0.14 ± 0.04	0.98 ± 0.01	2.55 ± 0.06		6.8 ± 0.9	11.2	7.6
S_0/L_1	0.6	2MV 60	4–11	23.6 ± 0.5	1.04 ± 0.01	0.05 ± 0.05	0.99 ± 0.01	3.15 ± 0.05	0.21 ± 0.03	7.5 ± 0.8	2.7	9.9
			63–90	22.1 ± 1.6	1.02 ± 0.01	0.21 ± 0.10	0.98 ± 0.01	2.64 ± 0.05		8.4 ± 0.9	7.4	7.6
S_0/L_1	0.7	2MV 70	4–11	25.6 ± 0.3	1.03 ± 0.01	0.07 ± 0.03	0.98 ± 0.01	2.88 ± 0.05	0.20 ± 0.03	8.9 ± 0.9	2.1	9.9
			63–90	26.6 ± 2.1	1.03 ± 0.01	0.09 ± 0.02	0.98 ± 0.01	2.41 ± 0.05		11.0 ± 1.2	8.1	7.6
S_0/L_1	0.8	2MV 80	4–11	31.2 ± 0.4	1.00 ± 0.01	0.07 ± 0.03	0.95 ± 0.01	2.81 ± 0.05	0.20 ± 0.03	11.1 ± 1.1	2.0	10.0
			63–90	36.4 ± 2.9	1.02 ± 0.01	0.09 ± 0.03	0.95 ± 0.01	2.35 ± 0.05		15.5 ± 1.7	8.2	7.6
S_0/L_1	0.9	2MV 90	4–11	35.9 ± 0.6	0.99 ± 0.01	0.19 ± 0.04	0.98 ± 0.01	2.77 ± 0.05	0.19 ± 0.03	12.9 ± 1.3	2.5	10.0
			63–90	36.0 ± 2.5	1.03 ± 0.01	0.05 ± 0.02	0.97 ± 0.01	2.32 ± 0.05		15.5 ± 1.6	7.2	7.6
S_0/L_1	0.93	MV 2.1	4–11	28.3 ± 0.6	1.04 ± 0.01	0.03 ± 0.03	0.94 ± 0.01	2.75 ± 0.04	0.19 ± 0.03	14.0 ± 1.4	2.3	9.7
			63–90	36.1 ± 2.0	1.02 ± 0.01	0.11 ± 0.03	0.98 ± 0.01	2.31 ± 0.04		15.6 ± 1.5	5.8	7.6
S_0/L_1	0.99	MV 2.2	4–11	51.7 ± 0.6	0.99 ± 0.01	0.04 ± 0.01	0.98 ± 0.01	2.88 ± 0.05	0.19 ± 0.03	18.0 ± 1.8	2.2	9.7
			63–90	53.6 ± 2.6	1.01 ± 0.01	0.04 ± 0.02	0.97 ± 0.01	2.42 ± 0.05		22.1 ± 2.1	5.2	7.7
S_0/L_1	1.23	MV 2.3	4–11	51.2 ± 0.9	1.02 ± 0.02	0.04 ± 0.02	0.90 ± 0.01	2.81 ± 0.06	0.18 ± 0.03	18.2 ± 1.9	2.8	9.9
			63–90	62.1 ± 3.0	1.01 ± 0.01	0.15 ± 0.07	0.97 ± 0.01	2.53 ± 0.05		26.4 ± 2.5	5.3	7.6
S_0/L_1	1.35	MV 2.4	4–11	46.8 ± 0.8	1.03 ± 0.02	0.04 ± 0.02	0.98 ± 0.01	2.92 ± 0.04	0.18 ± 0.03	16.1 ± 1.6	2.2	9.9
			63–90	60.8 ± 3.8	1.02 ± 0.01	0.09 ± 0.03	0.97 ± 0.01	2.44 ± 0.04		24.9 ± 2.5	6.4	7.7
S_0/L_1	1.47	MV 2.5	4–11	59.7 ± 1.0	1.03 ± 0.01	0.04 ± 0.02	0.92 ± 0.01	2.85 ± 0.05	0.18 ± 0.03	20.9 ± 2.1	2.3	9.9
			63–90	79.0 ± 4.1	1.00 ± 0.01	0.06 ± 0.02	0.97 ± 0.01	2.39 ± 0.04		33.1 ± 3.1	5.5	7.7
S_0/L_1	1.67	MV 2.6	4–11	67.4 ± 0.6	1.00 ± 0.01	0.05 ± 0.01	0.98 ± 0.01	2.91 ± 0.05	0.17 ± 0.03	22.8 ± 2.3	2.0	10.1
			63–90	86.9 ± 3.5	1.00 ± 0.01	0.06 ± 0.03	0.98 ± 0.01	2.42 ± 0.04		35.9 ± 3.2	4.4	7.7
L_2	5.70	2MV 570A	4–11	331 ± 6	0.96 ± 0.01	0.10 ± 0.01	0.95 ± 0.01	3.03 ± 0.06	0.11 ± 0.02	109 ± 11	2.6	10.0
			63–90	303 ± 13	0.97 ± 0.01	0.06 ± 0.02	0.96 ± 0.01	2.54 ± 0.05		120 ± 11*	4.7	7.8
L_2	5.70	2MV 570B	4–11	331 ± 3	0.96 ± 0.01	0.09 ± 0.01	0.96 ± 0.01	2.95 ± 0.06	0.11 ± 0.02	112 ± 12	2.2	10.1
			63–90	353 ± 13	0.97 ± 0.01	0.05 ± 0.02	0.95 ± 0.01	2.46 ± 0.05		143 ± 13*	4.2	7.8
L_3	13.70	2MV L3A	4–11	514 ± 16	0.98 ± 0.01	0.06 ± 0.01	0.98 ± 0.01	2.88 ± 0.05	0.06 ± 0.01	179 ± 19	2.4	10.3
			63–90	475 ± 19	0.96 ± 0.01	0.010 ± 0.02	0.94 ± 0.01	2.39 ± 0.04		199 ± 18*	4.3	8.0
L_3	13.70	2MV L3B	4–11	501 ± 11	0.98 ± 0.01	0.05 ± 0.01	0.99 ± 0.01	2.86 ± 0.06	0.06 ± 0.01	175 ± 18	2.2	10.2
			63–90	501 ± 23	0.95 ± 0.01	0.11 ± 0.02	0.94 ± 0.01	2.38 ± 0.05		210 ± 20*	5.0	8.0
L_4	17.70	2MV L4A	4–11	567 ± 9	0.99 ± 0.01	0.05 ± 0.002	1.00 ± 0.01	3.14 ± 0.05	0.04 ± 0.01	180 ± 19	2.3	10.4
			63–90	577 ± 23	0.97 ± 0.01	0.13 ± 0.02	0.97 ± 0.01	2.60 ± 0.05		222 ± 20*	-	-
L_4	17.70	2MV L4B	4–11	477 ± 6	1.00 ± 0.01	0.07 ± 0.004	0.91 ± 0.01	3.41 ± 0.06	0.04 ± 0.01	140 ± 13	2.2	8.8
			63–90	555 ± 26	0.98 ± 0.01	0.17 ± 0.03	0.95 ± 0.01	2.31 ± 0.05		240 ± 23*	-	-
L_5	20.50	2MV L5A	4–11	566 ± 8	0.98 ± 0.01	0.07 ± 0.003	0.98 ± 0.01	2.66 ± 0.06	0.04 ± 0.01	213 ± 22	2.5	10.2
			63–90	425 ± 39	0.98 ± 0.01	0.21 ± 0.09	0.98 ± 0.01	2.22 ± 0.05		192 ± 24*	-	8.0
L_5	20.50	2MV L5B	4–11	556 ± 13	0.99 ± 0.01	0.06 ± 0.01	0.98 ± 0.01	2.98 ± 0.06	0.04 ± 0.01	187 ± 20	2.9	-
			63–90	443 ± 35	0.94 ± 0.02	0.43 ± 0.10	0.97 ± 0.03	2.48 ± 0.05		179 ± 20*	8.1	8.0

3.1.4. Ages and discussion

Previous luminescence dating studies on Mircea Vodă site (**Figure 3.1.2a**) revealed an age discrepancy between the two quartz fractions investigated that is still not yet understood. Despite the fact that both datasets were consistent with the stratigraphic position of the samples, the fine (4–11 μm) quartz ages for the three samples taken from the L_2, L_3 and L_4 loess units were interpreted as underestimates. The post-IR IR_{225} signal was considered more reliable than the previously obtained quartz ages for the L_2, L_3 and L_4 units. These ages are presented alongside the quartz ages in **Figure 3.1.2a**.

For the current research, fine (4–11 μm) and coarse (63–90 μm) quartz have been investigated by applying SAR-OSL protocol in order to augment the existing chronological framework from Mircea Vodă loess-paleosol master section. The age results for the Pleistocene/Holocene transition have shown that fine and coarse fractions agree only up to ~20 ka (**Figure 3.1.2b)**. For samples older than this, fine grains quartz ages underestimate coarse quartz ages. Thus, the discrepancy between two datasets occurs sooner than previously shown for other sites (Timar-Gabor et al., 2017). The reason for this difference is yet not understood.

As previously reported, the 63–90 μm quartz does not underestimate the expected geological ages and agrees with post-IR IR_{225} for samples collected just below S_1. For older samples coarse quartz SAR-OSL signals approach (86%) laboratory saturation and also enter field saturation. For the counterpart fine grains quartz OSL natural signals are significantly below laboratory saturation levels. However, the fine quartz ages underestimate the expected ages. Therefore, these ages should be taken as minimum ages. Investigation on extended growth curves up to 5 kGy (for 4–11 μm quartz grains) and 2 kGy (for 63–90 μm quartz grains) using test doses of a different order of magnitude (17 and 170 Gy) have concluded that the equivalent dose was insensitive to the size of the test dose.

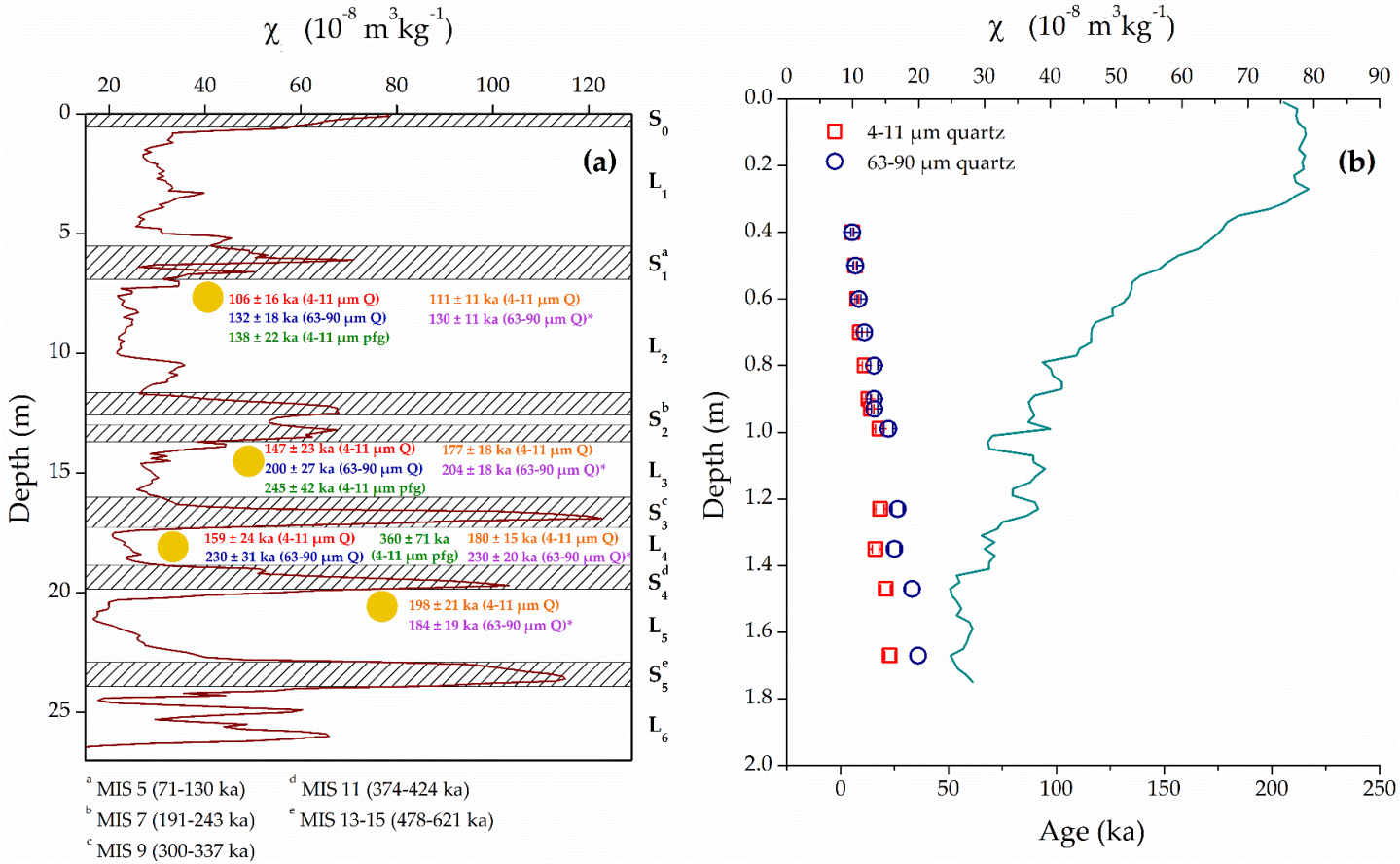

Figure 3.1.2. (**a**) Schematic representation of the loess (L) and paleosol units (S; hatched area) with magnetic susceptibility values (χ) from Timar-Gabor et al. (2011). The boundaries of paleosols developed during odd marine isotope stages (MIS) are after Lisiecki and Lisiecki (2002). The ages for the old samples and new samples are shown as follows: written in red - Timar et al. (2010); blue - Timar-Gabor et al. (2011); green - Vasiliniuc et al. (2012); orange – fine (4–11 μm) quartz, current study; purple coarse (63–90) μm quartz, current study. The new OSL ages represent the weighted results from the doublet samples and the ones marked with asterisk (*) were obtained for samples which were found to be close to saturation levels. (**b**) Plot of new optical ages (from S_0 and L_1) units as a function of depth alongside new magnetic susceptibility data. The fine (4–11 μm) quartz ages are represented as open squares and the coarse (63–90 μm) quartz ages are represented as open circles.

3.2. Preliminary optically stimulated luminescence study on the Pleistocene/Holocene transition as recorded in loess-paleosol sequences from the Lower Danube Basin

3.2.1. Introduction

With loess-paleosol sequences representing important archives of Quaternary environmental changes, establishing a robust chronology and reliable reconstruction of the past is often achieved by involving multi-proxy analysis. The transition between Pleistocene and Holocene has been dated 11.7 ka ago according to the layer-counted GICC05 timescale, while the radiocarbon-dated regional benthic $\delta^{18}O$ stacks from the North Atlantic dated the event at ~ 17 ka (Stern and Lisiecki, 2014). The fact that the synchronicity assumption does not stand even for recent climatic transitions implies a reassessment of the "wiggle matching" trend (e.g. Marković et al., 2015).

Two LPSs from the Lower Danube Basin in SE Europe, Mircea Vodă and Râmnicu Sărat were selected for assessing the synchronicity of the regional response to the last glacial-interglacial transition as recorded in marine and ice core records. The two sites were investigated in what regards optically stimulated luminescence and magnetic susceptibility.

3.2.2. Study site and sampling

The Râmnicu Sărat section (45° 41′ N, 27° 02′ E) has not been as intensely studied as Mircea Vodă. The 186 m thick section is situated on the left bank of the Râmnicu Sărat river valley and displays only three pedocomplexes overlying fluvial gravel. Previous proxy investigations have been carried out for mineralogical, grain-size, magnetic and geochemical analysis by Dimofte (2012). A total of 12 samples were collected covering the top 1.6 m from Râmnicu Sărat section, including the visual transition between L_1 and S_0. The samples were taken at a resolution of 5 cm from a cleaned outcrop, using stainless steel tubes. A gradual color change from L_1 loess to S_0 soil was observed at a depth ranging from 1.1 to 1.3 m.

3.2.3. Optical dating

3.2.3.1. Sample preparation, analytical facilities, and measurement protocols

The coarse (63–90 μm) quartz fraction has been obtained using standard laboratory preparation under red light conditions. The material from the end of each sample tube was used for magnetic analysis (Constantin et al., 2019). All luminescence measurements were performed using Risø TL/OSL-DA-20 readers (Thomsen et al., 2006). The SAR protocol was used for determining the ED for coarse (63–90 μm) quartz fraction (Murray and Wintle, 2000, 2003). The radionuclide specific activities were

determined though high-resolution gamma spectrometry using a well type high purity germanium detector.

3.2.3.1. Preheat plateau

In order to verify the most suitable thermal pretreatment for the Râmnicu Sărat samples, the dependency of ED on the preheat treatment was assessed for RS 090A and RS 160 .The samples showed no systematic variation in the ED for the 200 – 280 °C preheat temperature range, with recycling ratios close to unity and recuperation negligible compared to the natural signal. No temperature dependence has also been observed between the 180 °C and the 220 °C cutheats employed.

3.2.3.2. Equivalent dose determination

At least 10 aliquots have been measured for each sample as to determine the equivalent doses (**Table 3.2.1**).

3.2.3.3. Dose recovery test

Dose recovery tests (Murray and Wintle, 2003) were carried out on the coarse (63-90 μm) quartz fraction for samples RS 100A, 120, 150 and 160. Two samples (RS 090 and RS 160) have been additionally tested by using a 180/160 °C preheat/cutheat combination. The second thermal treatment combination did not influence the recovered dose, with good agreement between the dose recovery ratios.

3.2.4. OSL ages and discussion on assessing the Pleistocene/Holocene transition

The optical ages and uncertainty calculation are presented in **Table 3.2.1**. The approach used to define the threshold of the transition for the MS data was similar to that of Constantin et al. (2019) and analogous to that of Stern and Lisiecki (2014) (**Figure 3.2.1**). Low-field magnetic susceptibility (χ_{lf}) and frequency dependent magnetic susceptibility (χ_{fd}) were taken into consideration as paleoclimate proxies for the two sections. The onset of the transition was constrained at the depth for which both χ_{lf} and χ_{fd} values recorded the highest and most continuous increase in comparison to the values that characterize the L_1 loess. The time variation of the MS record across the Pleistocene/Holocene transition is synchronous for Mircea Vodă and Râmnicu Sărat loess-paleosol sites. The onset of increase of the magnetic susceptibility signal started closer to the 17-ka transition from the radiocarbon-dated regional benthic $\delta^{18}O$ stacks (Stern and Lisiecki, 2014) and earlier than the 11.7 ka stratigraphic transition from the ice core records. It also appears that the MS behavior for the sites investigated echo a gradual Pleistocene/Holocene transition. These observations are similar to the results reported on two other sites by Constantin et al. (2019) – Roxolany

(Ukraine) and Mošorin (Serbia). Moreover, pedogenesis and dust sedimentation appear to operate simultaneously, leading to the formation of accretional Holocene soils in the sites investigated.

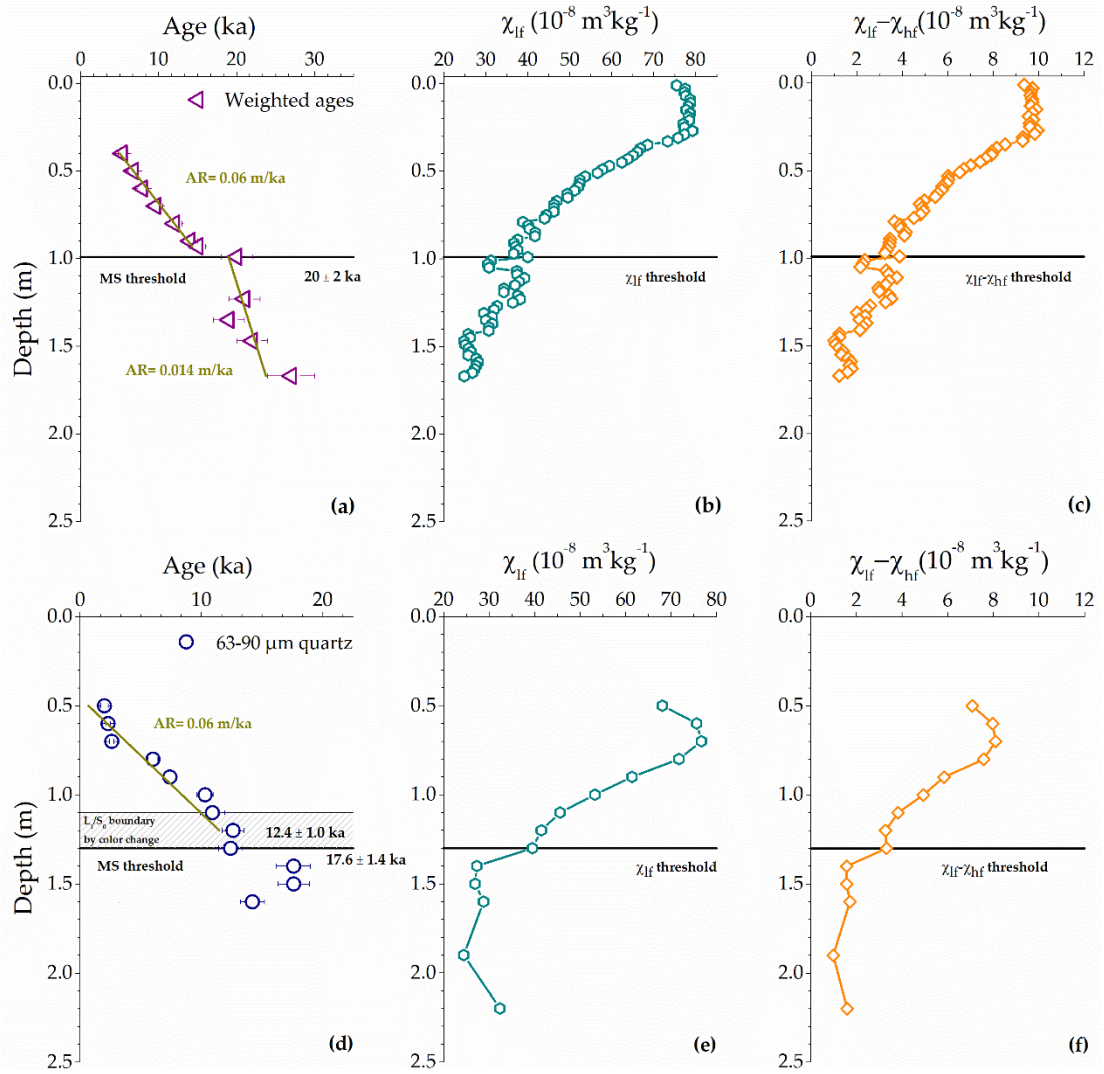

Figure 3.2.1. Quartz OSL ages displayed as a function of depth for Mircea Vodă **(a)** and Râmnicu Sărat **(d)**. For Mircea Vodă, the weighted average ages were obtained according to Aitken (1985) based on results from fine (4-11 µm) and coarse (63-90 µm) quartz. For Râmnicu Sărat the coarse (63-90 µm) quartz ages are presented. Sediment accumulation rates (AR) were obtained using linear regression of the OSL ages with depth (**a, c**). Details regarding the MS threshold is given in the text. The L_1/S_0 boundary identified in the field is shown for reference. Low frequency and frequency dependence MS curves are shown for Mircea Vodă **(b, c)** and Râmnicu Sărat **(e, f).**

Table 3.2.1 . Equivalent doses (ED), dosimetry measurements and OSL ages for Râmnicu Sărat samples. Water content estimation was based on the difference between the 'as found' and oven-dried weight of the material. The uncertainties associated with luminescence and dosimetry data are random. The uncertainties associated with the optical ages represent the overall uncertainties. The relative systematic errors taken into account include: 2% beta source calibration, 3% conversion factors, 5% attenuation and etching factors, 3% gamma spectrometer calibration, 15 % cosmic radiation, 25 % water content. All the errors correspond to 1σ. The letter 'n' denotes the number of accepted aliquots.

verifi	Depth (m)	Water content (%)	Grain size (μm)	ED (Gy)	U-Ra (Bq/kg)	Th (Bq/kg)	K (Bq/kg)	Total dose rate (Gy/ka)	Total random error (%)	Total systematic error (%)	Age (ka)
RS 050	0.5	4%	63-90	5.2 ± 0.6 n=11	33.6 ± 1.7	32.1 ± 0.8	380.8 ± 11.9	2.61 ± 0.05	11.7	5.4	2.0 ± 0.3
RS 060	0.6	2%	63-90	6.9 ± 0.4 n=11	35.7 ± 2.2	35.5 ± 0.4	457.9 ± 13.6	3.02 ± 0.06	6.1	5.4	2.3 ± 0.2
RS 070	0.7	9%	63-90	7.3 ± 0.3 n=9	35.8 ± 1.0	34.2 ± 1.9	468.4 ± 13.9	2.79 ± 0.05	4.5	5.9	2.6 ± 0.2
RS 080	0.8	5%	63-90	16.8 ± 0.5n=11	34.6 ± 1.4	33.3 ± 1.7	446.5 ± 11.9	2.81 ± 0.05	3.5	5.5	6.0 ± 0.4
RS 090	0.9	2%	63-90	23.4 ± 0.7 n=18	37.6 ± 0.2	38.4 ± 1.3	489.2 ±15.1	3.18 ± 0.05	3.4	5.4	7.4 ± 0.5
RS 100	1.0	6%	63-90	29.7 ± 1.0 n=20	35.8 ± 1.6	37.5 ± 1.4	459.0 ± 12.9	2.90 ± 0.05	3.8	5.6	10.3 ± 0.7
RS 110	1.1	6%	63-90	32.7 ± 2.1 n=11	36.4 ± 1.4	39.6 ± 0.6	482.9 ± 13.4	3.01 ± 0.05	6.6	5.6	10.9 ± 1.0
RS 120	1.2	6%	63-90	37.1 ± 1.4 n=19	37.0 ± 1.7	41.3 ± 3.2	450.0 ± 15.3	2.95 ± 0.08	4.6	5.6	12.6 ± 0.9
RS 130	1.3	5%	63-90	36.0 ± 1.9 n=14	36.7 ± 1.3	38.1 ± 1.8	447.7 ± 15.9	2.92 ± 0.06	5.7	5.5	12.4 ± 1.0
RS 140	1.4	9%	63-90	42.4 ± 1.7 n=15	32.5 ± 2.4	33.6 ± 3.0	367.8 ± 14.7	2.41 ± 0.07	5.0	5.9	17.6 ± 1.4
RS 150	1.5	6%	63-90	50.4 ± 1.9 n=15	33.9 ± 1.4	35.4 ± 1.4	475.8 ± 18.1	2.86 ± 0.06	4.4	5.6	17.6 ± 1.3
RS 160	1.6	6%	63-90	37.6 ± 1.3 n=14	35.9 ± 3.3	35.5 ± 3.0	394.2 ± 15.6	2.66 ± 0.08	4.7	5.6	14.2 ± 1.0

3.3. Optically stimulated luminescence dating of the Holocene (S_0) soil from Luochuan master section, China – preliminary results

3.3.1. Introduction

The Chinese Loess Plateau (CLP) represents an almost continuous and complete record of terrestrial sedimentation for the past 2.6 Ma. Recent research has raised the question of erosional events due to ice-volume-forced processes across the plateau (Stevens et al., 2018; H. Lu et al., 2006). Discontinuities in the sedimentary record can have serious implication for the interpretation of climate proxies and these have already been reported at the Luochuan section (H. Lu et al., 2013) close to L_1/S_0 transition. In this regard, high-resolution luminescence dating and multi-proxy analyses on the Pleistocene/Holocene transition were performed at the Luochuan master section in order to augment the existing chronological data and to check possible effects of erosional events.

3.3.2. Study site and samples

Luochuan (35°45′N, 109°25′E) loess-paleosol sequence is considered a standard pedostratigraphic section of the CLP in China and a key section for paleoclimate research (e.g. Kukla and An, 1989; Porter and An, 1995; Heller and Evans, 1995; Bronger, 2003). The 135 m thick section comprises more than 30 loess-paleosol alternations (Gallet et al., 1996). A chronological framework for Luochuan was also obtained through luminescence methods. Thermoluminescence ages were reported by Forman (1991). Optically stimulated results were reported by Y.C. Lu et al. (2007), Li and Li (2012), Fu et al. (2012), Lai (2010), Lai and Fan (2014) and H. Lu et al (2013).

Part of a new sampling campaign intends to revisit the chronology at Luochuan, covering the entire Holocene soil (S_0) and the top of L_1. Hence, in addition to new magnetic susceptibility and grain size samples, 25 samples have been collected.

3.3.3. Optical dating

3.3.3.1. Sample preparation, analytical facilities, and measurement protocols

Sample preparation alongside radionuclide and OSL measurements were underwent at the Nordic Laboratory for Luminescence Dating in Roskilde, Denmark, during a 3-month research stage. Standard laboratory preparation was followed for extracting the coarse (63–90 μm) quartz from the 25 samples. All luminescence measurements were performed using Risø TL/OSL-DA-20 readers (Thomsen et al., 2008). The radionuclide specific activities were determined through high-resolution gamma spectrometry using a well type-high purity germanium detector. For higher-

precision natural dose rate estimation, the beta counting method (Cunningham et al., 2018) was also used.

3.3.3.2. Equivalent dose determination

In order to determine the ED, a minimum of 19 aliquots have been measured for each of the 25 samples.

3.3.3.3. Dose recovery test

In order to assess whether the SAR protocol manages to successfully correct the sensitivity changes that occur during measurement cycles, dose recovery test (Murray and Wintle, 2003) were carried out on the coarse (63-90 μm) quartz fraction for all samples with the exception of the first four. Twelve samples exhibit ratios underestimated by 11 and 15%.

3.3.4. OSL ages and preliminary results

The natural dose rate has been obtained using both high-resolution gamma spectrometry and beta counting; both analytical methods gave indistinguishable results for the beta dose rate component. As a result, the OSL ages were further calculated using the radionuclide concentration obtained through high-resolution gamma spectrometry. The age results on coarse (63-90 μm) generally increase with depth (**Figure 3.3.1**). However, multiple inversions are observed which are not related to the dose rate values, but rather to the equivalent doses. Therefore, the relative overdispersion (OD) in individual multigrain ED data was calculated in R Package Luminescence by applying the Central Age Model after Galbraith et al. (1999) (Burrow, 2020). The OD values generally revolve around 20%.

Despite the fact that no hiatuses were noted, the presence of highly variable OSL ages is similar to reports from Xifeng and Shiguazhai (Stevens et al., 2007b) but appear to occur sooner. The variation could be accounted for pedogenic disturbance or non-eolian deposition such as colluvial, alluvial or mass wasting processes (Stevens et al., 2007b). Pedogenic processes during the formation of the S_0 soil extended into L_1 has been already shown to impact the loess-paleosol records from the Loess Plateau by OSL dating (Lai and Wintle, 2006; Stevens et al., 2006).

The overall ages strongly indicate towards a significant vertical mixing over time while implicitly assuming a top-down pedogenesis model (Bateman, 2003; Jacobs and Mason, 2007).

Figure 3.3.1. Dosimetry, dose rates, equivalent doses and OSL ages for all 25 samples collected from Luochuan loess-paleosol sequence. The K, Th and U specific activities presented in this figure have been obtained using high resolution gamma spectrometry. The dose rates for the sand-sized (63-90 μm) quartz and have been calculated based on the conversion factors derived from Guérin et al. (2011). The beta attenuation and etching factor for the 63–90 μm fraction was assumed to be 0.94 ± 0.04 (Mejdahl, 1979). The water content was taken as being 15%. The total dose rate includes the external contribution from beta and gamma radiation, as well as the cosmic ray contribution. The cosmic ray dose rate was estimated for each sample as a function of depth, altitude, and geomagnetic latitude (Prescott and Hutton, 1994).

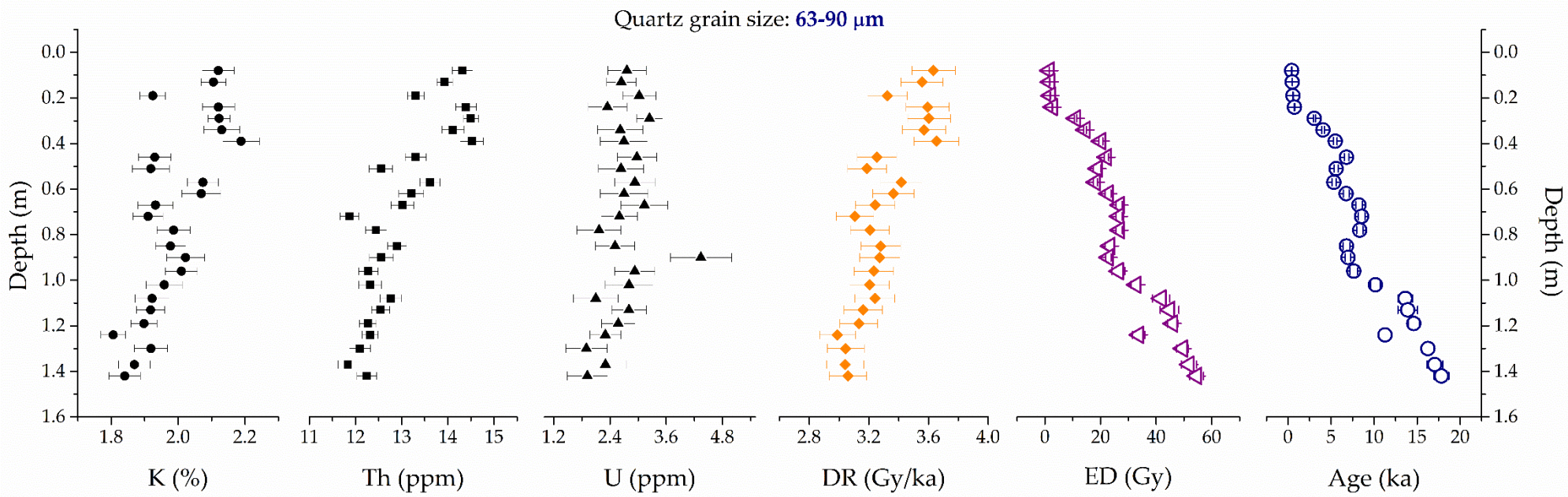

4. OPICALLY STIMULATED LUMINESCENCE INVESTIGATIONS IN LOESS-PALEOSOL SITES FOR THEIR ARCHEOLOGICAL IMPORTANCE

4.1. Optically stimulated luminescence ages for the Upper Palaeolithic site Krems-Wachtberg

4.1.1. Introduction

The Upper Paleolithic site cluster of Krems is located in eastern Austria, a region known for important archeological profiles such as Stillfried, Willendorf, Krems-Hundssteig and, most recently, Krems-Wachtberg. Recent excavations exposed part of a Gravettian living floor with hearths, pits, and infant burials (Einwögerer et al., 2006; Händel et al., 2009). These evident structures, together with the rich find assemblages are excellently preserved due to the embedment in a thick loess accumulation.

4.1.2. Study site and sampling

The Krems-Wachtberg site (48°24'N/15°35'E) is located in Lower Austria near the confluence of the Danube and Krems rivers. The stratigraphy of previously studied profile from the site reveals a generally continuous 8 m thick loess sequence. In the northern part of the excavated area, the main Gravettian find layer AH4 is embedded 5.5 m beneath the surface (Händel et al., 2009). Within the sequence, specific geological horizons (GH) have been defined by sedimentological properties, while archeological horizons (AH) are defined by the presence of anthropogenic material (Händel et al., 2014). In the current study 16 samples have been analyzed from three profiles.

4.1.3. Analytical facilities and measurement protocols

Luminescence measurements were carried out using Risø TL/OSL-DA-20 readers. Luminescence investigations were carried out using the single-aliquot regenerative dose (SAR) protocol for the fine (4-11 μm) and coarse (63-90 μm) fractions (Murray and Wintle, 2000; 2003). The Krems-Wachtberg samples were investigated for assessing the purity of the quartz extracts using scanning electron microscopy (SEM). Elemental identification and quantitative compositional information were obtained using energy dispersive X-ray spectroscopy (EDX). High resolution gamma spectrometry was carried out. Susceptibility measurements were undertaken on samples collected for palaeomagnetic analyses.

4.1.4. Optical dating

4.1.4.1. Sample preparation

Standard laboratory sample preparation procedures have been followed. Despite the chemical treatment applied, poor results were obtained in preliminary OSL investigations on fine grains. Consequently, another batch of fine fraction (4-11 μm) material was obtained for all 16 samples and an extended 20 days H_2SiF_6 attack treatment was performed. To further assess the purity of quartz grains for both fractions, SEM and EDX analysis has been performed on three samples. The results concluded the fact that the material contains, besides quartz, a rather significant amount of minerals which are especially rich in Al, Fe and Ti.

4.1.4.2. Equivalent doses – luminescence characteristics and behavior

4.1.4.2.1. Continuous wave OSL

The performance of the SAR protocol applied was tested in terms of recycling, IR depletion and recuperation (Murray and Wintle, 2003). Despite extensive sample preparation and repeated measurements, SAR intrinsic rigor tests raised significant issues. The application of the rejection criteria of SAR protocol resulted in reducing the relative standard deviation of the equivalent doses with values ranging from 5 to 21% in the case of fine grains (4-11 μm) and from 10 to 28% in the case of coarse (63-90 μm) grains, respectively. However, the application of these rejection criteria did not actually result in a significant change in the average EDs.

4.1.4.2.2. Dose recovery

Dose recovery tests (Murray and Wintle, 2003) were carried out on 4-11 μm and 63-90 μm quartz grains from KWA 025 to KWA 467.5 and 487.5, respectively. For the fine (4-11 μm) quartz fraction, the recovered to given dose ratios are underestimating with 2-9%. For the coarse (63-90 μm) fraction, samples KWA 175 and 462.5 ratios of unity have been obtained. For the rest of the samples the recovered to given dose ratios vary from unity with 2-7%, except for KWA 325 for which the ratio exceeds the 10% threshold, an overestimation of 11% being determined.

4.1.4.2.3. Pulsed OSL

Taking into consideration the highly contaminated material, attempts have been made in order to better separate quartz OSL signals using pulsed stimulation (POSL). Comparing the behavior of the analyzed aliquots in the SAR protocol using POSL and standard CW-OSL if all measured aliquots were considered (both fine (4-11 μm) and coarse (63-90 μm) quartz), an improvement in the acceptance rate could

be observed in the case of the application of the POSL protocol, with 68% (87% for fine grains and 51% for coarse grains, respectively) accepted aliquots compared to 48% (64% for fine grains and 43% in for coarse grains, respectively) accepted aliquots in standard CW-OSL measurements. However, as in the case of employing the rejection criteria, by applying the two different stimulation methods, no significant changes could be observed in the average values for the equivalent doses.

4.1.4.2.4. Dose response curves saturation characteristics

For sample KWAK 575, CW-OSL (4-11 μm quartz grains) and POSL (63-90 μm quartz grains) sensitivity corrected growth curves up to 5 kGy were constructed. The extended dose response curves confirm the different saturation characteristics between coarse and fine quartz in the high dose range, with the fine fraction saturating at higher doses (D_{01}= 97 Gy; D_{02}=1101 Gy) than the coarse grains (D_{01}= 50 Gy; D_{02}=755 Gy). Also, as previously reported (Timar-Gabor et. al, 2017), the dose response curves are overlapping up to doses of about 100 Gy.

4.1.4.2.5. Influence of different thermal treatments

Additionally, different thermal treatments have been tested during POSL measurements on coarse (63-90 μm) extracts for three samples. The equivalent doses obtained using these different thermal treatments are consistent within errors, thus the effect of using different preheat and cutheat treatments does not result in significantly different equivalent doses.

4.1.4.3. Optical ages

Optical ages obtained using the equivalent doses determined via CW-OSL and POSL are presented in **Table 4.1.1** and plotted as function of depth in relationship to the geological horizons in **Figure 4.1.1**. Agreement between the ages obtained using SAR-OSL on fine (4-11 μm) and coarse (63-90 μm) quartz extracted from loess for equivalent doses in the range of the equivalent doses obtained in this study (i.e. less than 100-150 Gy) has been previously reported on other sites as well (Constantin et al, 2012; Timar-Gabor et al., 2017).

Table 4.1.1. Environmental activity and OSL dating results. The number of accepted aliquots out of the total measured is indicated in the subscript to the ED data. The uncertainties indicated along with the luminescence and dosimetry data are random and the uncertainties mentioned with the optical ages are the overall uncertainties. All uncertainties represent 1σ. The total dose rate includes the contribution from cosmic rays (Prescott and Hutton, 1994), from gamma, beta and alpha (for 4-11μm quartz grains) radiations, as well as the internal contribution for the coarse (63-90 μm) fraction (assumed to be 0.01 Gy/ka). Beta attenuation and etching factor for 63-90 μm quartz grains was assumed to be 0.94 ± 0.047 (Mejdahl, 1979) and the alpha efficiency factor considered was 0.04 ± 0.02 (Rees-Jones and Tite, 1997). Water content was based on the difference between the natural "as found" and the oven-dried weight of the material. Water content values ranged from 8 to 20%. Overdispersion has been calculated and values have been obtained ranging from 2% to 18% in the case of fine grains (4-11 μm) and from 3% to 31% for coarse grains (63-90 μm).

Horizon no.	Depth (m)	Sample code	Luminescence method	Quartz fraction	ED (Gy)	U (ppm)	Th (ppm)	K (%)	Total dose rate (Gy/ka)	Total random error (%)	Total systematic error (%)	Age (ka)
GH 5	0.25	KWA 025	CW-OSL	4-11 μm	$59.5 \pm 0.9_{12/13}$	2.66 ± 0.05	9.0 ± 0.1	1.04 ± 0.01	2.76 ± 0.02	1.9	9	22.0 ± 2.0
				63-90 μm	$-_{0/6}$				-	-	-	-
GH 7	0.75	KWA 075	CW-OSL	4-11 μm	$60.2 \pm 1.0_{10/11}$	2.60 ± 0.05	7.8 ± 0.07	1.03 ± 0.01	2.44 ± 0.02	1.6	9.8	25.0 ± 2.5
				63-90 μm	$51.8 \pm 3.4_{10/16}$				2.05 ± 0.01	6.6	7.5	25.3 ± 2.5
			POSL	63-90 μm	$51.1 \pm 5.3_{5/10}$				2.05 ± 0.01	10.4	7.5	24.9 ± 3.2
GH 9	1.25	KWA 125	CW-OSL	4-11 μm	$63.5 \pm 1.5_{8/10}$	2.68 ± 0.01	7.2 ± 0.2	1.02 ± 0.02	2.48 ± 0.02	2.3	9.2	28.1 ± 3.2
				63-90 μm	$51.9 \pm 4.9_{11/12}$				2.08 ± 0.02	9.5	6.8	25.0 ± 2.9
			POSL	4-11 μm	$50.4 \pm 1.7_{10/10}$				2.48 ± 0.02	3.5	9.2	20.3 ± 2.0
				63-90 μm	$46.9 \pm 2.4_{9/10}$				2.08 ± 0.02	5.2	6.8	22.6 ± 1.9
GH 11	1.75	KWA 175	CW-OSL	63-90 μm	$70.7 \pm 2.8_{11/15}$	2.91 ± 0.03	8.6 ± 0.2	1.15 ± 0.01	2.25 ± 0.02	4	7.4	31.5 ± 2.7
			POSL	63-90 μm	$68.2 \pm 4.3_{8/10}$					6.3	7.4	30.4 ± 3.0
GH 14	2.25	KWA 225	CW-OSL	4-11 μm	$89.0 \pm 2.4_{10/18}$	3.24 ± 0.04	9.9 ± 0.12	1.31 ± 0.02	3.17 ± 0.02	2.8	9.2	28.1 ± 2.7
				63-90 μm	$73.0 \pm 2.5_{10/28}$				2.64 ± 0.02	3.5	6.6	27.7 ± 2.1
GH 17	2.75	KWA 275	CW-OSL	63-90 μm	$70.0 \pm 2.7_{10/17}$	2.76 ± 0.05	8.6 ± 0.07	1.06 ± 0.01	2.21 ± 0.02	3.9	6.7	31.7 ± 2.5
GH 18	3.25	KWA 325	CW-OSL	63-90 μm	$71.2 \pm 3.4_{10/21}$	2.93 ± 0.05	8.7 ± 0.14	1.31 ± 0.02	2.43 ± 0.02	4.8	7	29.3 ± 2.5
GH 20	3.75	KWA 375	CW-OSL	63-90 μm	$70.8 \pm 2.3_{10/25}$	3.03 ± 0.11	9.1 ± 0.23	1.27 ± 0.02	2.44 ± 0.03	3.4	7	29.1 ± 2.3

GH 22	4.25	KWA 425	CW-OSL	4-11 μm	97.0 ± 1.4$_{10/16}$	3.02 ± 0.02	10.4 ± 0.12	1.39 ± 0.02	3.16 ± 0.02	1.6	9.2	30.7 ± 2.9
				63-90 μm	84.2 ± 3.7$_{11/28}$				2.64 ± 0.02	4.4	6.8	31.9 ± 2.6
GH 25	4.625	KWA 462.5	CW-OSL	4-11 μm	98.5 ± 0.9$_{24/32}$	3.08 ± 0.06	10.1 ± 0.29	1.42 ± 0.02	3.23 ± 0.03	1.4	8.9	30.5 ± 2.8
				63-90 μm	72.3 ± 8.1$_{4/14}$				2.70 ± 0.03	11.2	6.5	26.8 ± 3.5
			POSL	4-11 μm	95.3 ± 2.6$_{15/20}$				3.23 ± 0.03	2.9	8.9	29.5 ± 2.8
				63-90 μm	98.1 ± 11.0$_{4/20}$				2.70 ± 0.03	17.9	6.5	33.1 ± 6.3
GH 27	4.875	KWA 487.5	CW-OSL	4-11 μm	122.1 ± 3.4$_{10/20}$	3.15 ± 0.09	11.1 ± 0.25	1.56 ± 0.02	3.51 ± 0.04	3	8.8	34.8 ± 3.2
				63-90 μm	113.0 ± 5.4$_{3/14}$				2.93 ± 0.03	4.9	6.4	38.5 ± 3.1
			POSL	4-11 μm	67.0 ± 2.9$_{18/20}$				3.51 ± 0.04	4.4	8.8	19.1 ± 1.9
				63-90 μm	96.2 ± 9.7$_{10/20}$				2.93 ± 0.03	7.8	6.4	33.9 ± 3.4
GH 28	5.25	KWA 525	CW-OSL	4-11 μm	-$_{0/10}$	3.23 ± 0.01	11.0 ± 0.12	1.51 ± 0.02	-	-	-	-
				63-90 μm	-$_{0/14}$					-	-	-
GH 81	5.75	KWAK 575	CW-OSL	4-11 μm	81.3 ± 6.3 $_{7/14}$	3.39 ± 0.05	10.5 ± 0.07	1.58 ± 0.02	3.69 ± 0.02	-	-	22.0 ± 2.5
				63-90 μm	87.2 ± 4.1$_{10/21}$				3.07 ± 0.02	4.7	5.9	28.4 ± 2.1
GH 83	6.25	KWAK 625	CW-OSL	4-11 μm	110.5 ± 4.8$_{5/10}$	3.39 ± 0.09	10.0 ± 0.12	1.47 ± 0.05	3.31 ± 0.06	4.7	9.1	33.4 ± 3.4
				63-90 μm	109.5 ± 9.6$_{10/28}$				2.76 ± 0.05	9	6.7	39.7 ± 4.4
GH 85	6.75	KWAK 675	-	-	-	3.05 ± 0.03	9.2 ± 0.09	1.46 ± 0.02	-	-	-	-
GH 87.2	7.25	KWAK 725	POSL	4-11 μm	134.7 ± 3.1$_{9/10}$	3.11 ± 0.03	10.3 ± 0.25	1.83 ± 0.05	3.43 ± 0.05	2.8	9.3	39.2 ± 3.8

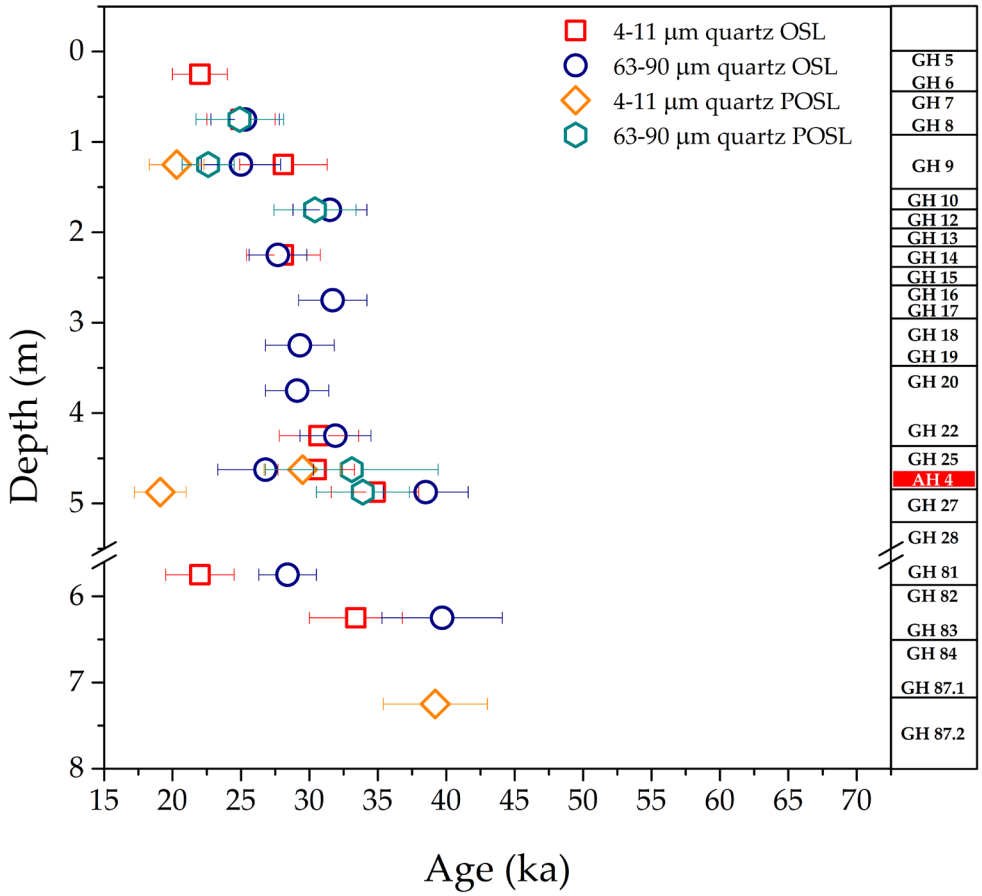

Figure 4.1.1. SAR CW-OSL and POSL ages plotted as function of depth and geological horizons (GH). Fine quartz ages are depicted as open squares, while coarse quartz ages are depicted as open circles. The errors bars on luminescence ages represent 1σ. The geological horizons are based on field observations and confirmed by magnetic susceptibility data.

4.1.5. Discussions and conclusion

The different thermal treatments that were carried out did not result in significant variations in the equivalent doses obtained and neither did the application of pulsed optically stimulated luminescence. The obtained chronological dataset confirms the previous assessment that the archive comprises Middle to Late Würmian loess (Hambach, 2010; Hambach et al., 2008; Händel et al., 2014). The arithmetic mean from all seven ages using different methods for the two samples collected above and below the main archeological layer AH4 is 32.4 ± 1.5 ka, thus agreeing within error limits with the results obtained by OSL and IRSL (Lomax et al., 2014), TL (Zöller et al., 2014) and radiocarbon (Einwögerer et al., 2009). Unfortunately, bearing in mind the difficulties encountered in the purification of quartz extracts and the poor behavior of the material in the SAR-OSL measurement protocol, obtaining a higher accuracy and precision for the chronology of Krems-Wachtberg site using currently available luminescence dating methods remains a challenging task, despite the archeological and paleoenvironmental significance of the site.

4.2. Kammern-Grubgraben revisited – First results from renewed investigations at a well-known LGM site in East Austria

4.2.1. Introduction

Up to this day, a limited number of stratified Upper Paleolithic sites dating to the LGM are known in Central Europe featuring well preserved occupational structures as well as considerable amounts of archeological materials. One such site is Kammern-Grubgraben, also referred to as "Grubgraben bei Kammern" or "Grubgraben". Extensive stone structures interpreted as dwellings have been uncovered alongside a considerably rich bone industry containing ivory points, needles with tiny eyes, spatulas and denticulated bone artifacts.

4.2.2. Study site and samples

The site Kammern-Grubgraben (48°28'28"N, 15°42'34"E) is located in Lower Austria, approximately 70 km west of Vienna. Here, a distinct loess-paleosol archive of approximately 9 m has been preserved in an extensive combe in the proximity of Kamp River, a tributary to the Danube. The open-air site of Grubgraben bei Kammern displays stratified archaeological deposits representing Late Paleolithic Epigravettian occupations as well as a high resolution paleoclimatic record. A new research reported by Händel et al. (2020) focused on obtaining new radiocarbon and OSL ages and analyzing the occupational sequence, settlement structure, economy, and mobility. In that respect, 10 doublet samples were recovered in 2015.

4.2.3. Optical dating

4.2.3.1. Samples preparation, analytical facilities, and measurement protocols

Standard sample preparation and luminescence investigation were carried out during one stage of research at the Nordic Laboratory for Luminescence Dating in Roskilde, Denmark. Due to the small sampling tubes and therefore low quantity of material, only the coarse (63-90 μm) quartz fraction was extracted. Luminescence measurements were performed using two automated Risø TL/OSL-DA-20 reader. The OSL measurements were carried out using the single-aliquot regenerative dose (SAR) protocol (Murray and Wintle, 2000, 2003). Radionuclide specific activities were measured by high-resolution gamma spectrometry in the Laboratory of Luminescence Dating and Dosimetry in Cluj-Napoca, Romania.

4.2.3.2. Equivalent doses - luminescence characteristics and behavior

For each investigated sample, between 12 and 22 replicate measurements of the equivalent dose were performed.

4.2.3.3. OSL ages

Data relevant to optical ages and uncertainty calculation are **Table 4.2.1**. The OSL ages as a function of depth are presented in **Figure 4.2.1**. In relation to their relative stratigraphic positions, samples ID 931, 932, 1482 and 1483 provided comparable chronologic results and which correspond to GS-3. This conclusion was also supported by radiocarbon ages which placed main occupation sequence AL2-4 posterior to GS-3. The samples located above AH102 (ID 1479 and 1480) and from the lowest position (ID 1485 and 1486) mark an earlier sedimentation episode which is unrelated to the archeological framework. Samples ID 1476 and 1477, taken from above AH101 were found to be in disagreement and displayed stratigraphical inversion.

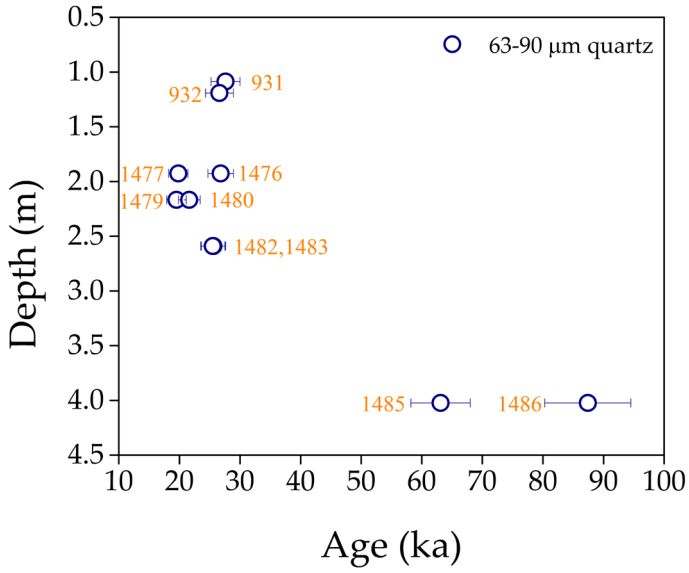

Figure 4.2.1. Depth versus OSL ages (calculated assuming water content of 15%).

Table 4.2.1. Summary of the luminescence and dosimetry data. The uncertainties associated with the luminescence and dosimetry data are random; the uncertainties mentioned with the optical ages are the overall uncertainties. All uncertainties represent 1σ. Specific activities were measured on well detector and the ages were determined considering a water content of 15%, with a relative error of 25%; n denotes the number of accepted aliquots; beta attenuation and etching factor used for 63-90 µm fractions is 0.94 ± 0.05. The total dose rate consists of the contribution from the beta and gamma radiations as well as the contribution from the cosmic radiation.

Sample code	Depth (m)	Grain size (μm)	Water content (%)	ED (Gy)	U-Ra (Bq/kg)	Th (Bq/kg)	K (Bq/kg)	Total random error (%)	Total systematic error (%)	Total dose rate (Gy/ka)	Age (ka)
931	1.087	63-90	15	78.2 ± 4.0 (n=11)	41.2 ± 1.1	68.3 ± 2.0	360.5 ± 10.2	5.3	6.0	2.984 ± 0.046	26.2 ± 2.1
932	1.192	63-90	15	58.4 ± 2.2 (n=8)	36.5 ± 0.4	34.8 ± 0.5	345.4 ± 11.0	4.0	6.1	2.307 ± 0.033	25.3 ± 1.9
1476	1.927	63-90	15	61.0 ± 2.2 (n=16)	40.1 ± 1.3	42.8 ± 0.8	318.2 ± 10.5	3.9	6.9	2.276 ± 0.036	26.8 ± 2.1
1477	1.927	63-90	15	53.2 ± 2.2 (n=17)	46.7 ± 2.4	49.8 ± 1.3	389.8 ± 10.2	4.5	7	2.694 ± 0.047	19.8 ± 1.6
1479	2.168	63-90	15	53.8 ± 1.8 (n=19)	53.5 ± 1.4	43.5 ± 1.6	408.1 ± 16.8	3.9	7	2.759 ± 0.055	19.5 ± 1.6
1480	2.168	63-90	15	54.1 ± 2.2 (n=19)	49.7 ± 1.1	39.2 ± 1.4	361.4 ± 10.3	4.3	7	2.500 ± 0.038	21.6 ± 1.8
1482	2.59	63-90	15	66.2 ± 2.0 (n=21)	45.1 ± 1.2	48.5 ± 0.5	371.5 ± 9.9	3.3	7	2.583 ± 0.032	25.6 ± 2.0
1483	2.59	63-90	15	66.5 ± 2.0 (n=21)	44.5 ± 0.9	47.6 ± 1.2	388.9 ± 10.1	3.3	7	2.606 ± 0.035	25.5 ± 2.0
1485	4.023	63-90	15	181.7 ± 5.1 (n=17)	43.8 ± 0.8	54.8 ± 2.1	458.1 ± 13.6	3.3	7.1	2.880 ± 0.050	63.1 ± 4.9
1486	4.023	63-90	15	233.0 ± 9.1 (n=20)	44.0 ± 0.8	47.2 ± 0.9	421.3 ± 10.4	4.1	7.1	2.666 ± 0.033	87.4 ± 7.1

4.2.4. Results and discussions

The scientific revisit at Kammern-Grubgraben managed to bring new insights to the results obtained by previous research. Based on the new OSL chronology, it is most probable that the AH2/102, corresponding to the main occupation layers AL2-4, can be placed from a chronostratigraphical point of view between the dust peaks at the end of GS-3 and onset of GS-2.1 sediment accumulation. Despite the connection with interstadial GI-2 (GI-2.2/GI-2.1), Händel al. (2020) disagrees with Haesaerts (1990) and Haesaerts and Damblon (2016) in what regards associating independent archeological layers to different interstadials, especially since the short time spans (ca. 120-200 yr) could not be accurately reported by radiometric or luminescence approaches. A clear distinction between GI-2.1 and GI-2.2 has not yet been successfully proven in regional loess sediment archives (Marković et al., 2015; Terhorst et al., 2015). Moreover, the dark bands believed to represent the two humic horizons contained no organic compounds (ash or humus), being interpreted as a result of disintegrated stone slabs and wind erosion (Händel et al., 2020).

The radiocarbon data and the archeological material recovered from the main occupation sequence AH2/102 (AL2-4) indicate that AH1/101 (AL1) represents a palimpsest of different occupations (Händel al., 2020). This interpretation is also supported by the slope processes observed in the area and the OSL chronology which yielded incongruent ages for the sediment above (ID 1476 and 1477). The redeposition due to erosion would also support the lack of three distinct occupations within AH2/102 (AL2-4), with the AL2a being most probably the result of post-occupational collapse and displacement (Händel al., 2020).

SUMMARY AND CONCLUSION

The new OSL investigations at Mircea Vodă on fine (4-11 μm) and coarse (63-90 μm) quartz from 21 new samples provided once more discrepancies between equivalent doses and ages, similar to previous reports on the matter (Timar-Gabor et al., 2011, 2012, 2015a; Constantin et al., 2014). However, in this case the difference occurs at ~20 ka, sooner than previously observed. Moreover, for older samples (starting from L_2 loess unit downwards) the same pattern of OSL ages underestimating true burial was observed, as reported by Timar-Gabor et al. (2011) and Vasiliniuc et al. (2012) at Mircea Vodă. In order to further investigate this behavior exhibited by the older samples, dose response curves (DRC) up to doses of 2 kGy (for 63-90 μm quartz) and 5 kGy (for 4-11 μm quartz) were constructed. Test doses of different order of magnitude (17 and 170 Gy) were employed in order to assess the closeness of the natural corrected luminescence signals to the saturation levels.

Moving on to the topic of assessing the Pleistocene/Holocene transition recorded in loess-paleosol sequences from the Lower Danube Basin in SE Europe, the results obtained from Mircea Vodă were compared to those from Râmnicu Sărat in what regards high-resolution OSL dating and magnetic susceptibility. The results confirmed a gradual S_0/L_1 transition placed at 20 ± 2 ka at Mircea Vodă and between 17.6 ± 1.4 ka and 12.4 ± 1.0 ka at Râmnicu Sărat. The dates for the Pleistocene/Holocene transition were further compared to those reported by Constantin et al. (2019). It can be concluded that the time variation of the MS record across the Pleistocene/Holocene transition is rather synchronous for all four sites, with the onset of increase of the magnetic susceptibility signal starting closer to the 17-ka transition from the radiocarbon-dated regional benthic $\delta^{18}O$ stacks (Stern and Lisiecki, 2014).

Situated in the famous Chinese Loess Plateau (CLP), Luochuan is one of the most intensely studied LPS, considered by many as a key section for paleoclimate research due to its over 30 loess-paleosol alternations. With recent concerns regarding the erosional events caused by ice-volume forced processes across the CLP, high-resolution luminescence dating on the Pleistocene/Holocene transition was performed during a 3-month research stage at the Nordic Laboratory for Luminescence Dating in Roskilde, Denmark. The most intriguing observation is that regarding the OSL ages which generally increase with depth but exhibit a worrying pattern with multiple inversions. The equivalent doses follow the same pattern, and the question is whether or not the issue is caused by significant vertical mixing.

The Krems-Wachtberg loess-paleosol site has been intensely studied, with a chronological framework being presented by Einwögerer et al. (2006, 2009), Lomax et

al. (2014), and Zöller et al. (2014). Due to both archeological and paleoenvironmental significance of the site, 16 new samples from three profiles have been analyzed in what regards OSL and MS. The process of extracting quartz grains from the samples proved to be a challenging task. Scanning electron microscopy (SEM) coupled with energy dispersive X-ray spectroscopy (EDX) analysis revealed the fact that even after extensive chemical treatments, the "quartz" material was highly contaminated with Fe, Al and TI rich minerals. Different thermal treatments and pulsed optically stimulated luminescence (POSL) were tested in order to improve ED determinations with no significant improvements. The different saturation characteristics of fine (4-11 μm) and coarse (63-90 μm) quartz fractions were investigated. The overall fine (4-11 μm) and coarse (63-90 μm) quartz ages were consistent, as expected for doses in the range of 100-150 Gy (Constantin et al., 2012; Timar-Gabor et al., 2017).

Last but not least, another chronological contribution to archeological studies was made in the case of the Kammern-Grubgraben site located also in Austria. The site is known not only for its rich bone history and occupation layers attributed to the Aurignacian culture, but also due to its intriguing paleoclimatic and geochronological interpretation. As a result, during a new field investigation 10 new samples have been collected. The ages obtained on coarse (63-90 μm) quartz grains proved once more the importance of OSL dating in establishing a robust chronology which, in this case, managed to clarify certain aspects regarding the complex stratigraphy of Kammern-Grubgraben.

All five loess-paleosol sites investigated in the current dissertation displayed a wide range of obstacles in what regards OSL dating on quartz, while at the same time providing methodological results and new chronologies which shed some light on previous research.

REFERENCES

1. Adamiec, G. 2000. Variations in luminescence properties of single quartz grains and their consequences for equivalent dose estimation. Radiation Measurements 32, pp. 427-432.
2. Adamiec, G. Aitken, M.J. 1998. Dose-rate conversion factors: new data. Ancient TL 16, pp. 37-50.
3. Anechitei-Deacu, V., Timar-Gabor, A., Fitzsimmons, K.E., Veres, D., Hambach, U. 2013. Multi-method investigations on quartz grains of different sizes extracted from a loess section in Southeast Romania interbedding the Campanian Ignimbrite ash layer. Geochronometria 41, pp. 1–14.
4. Bailey, R.M. 2001. Towards a general kinetic model for optically and thermally stimulated luminescence of quartz. Radiation Measurements 33, pp. 17-45.
5. Bailey, R.M., Smith, B.W., Rhodes, E.J. 1997. Partial bleaching and the decay form characteristics of quartz OSL. Radiation Measurements 27, pp. 123–136.
6. Bălescu, S., Lamothe, M., Panaiotu, C., Panaiotu, C. 2010. La chronologie IRSL des séquences loessiques de l'est de la Roumanie. Quaternaire 21, pp. 115–126.
7. Bateman, M.D., Frederick, C.D., Jaiswal, M.K., Singhvi, A.K. 2003. Investigations into the potential effects of pedoturbation on luminescence dating. Quaternary Science Reviews 22, pp. 1169–1176.
8. Berryman, K.R. 1993. Distribution, age, and deformation of Late Pleistocene marine terraces at Mahia Peninsula, Hikurangi subduction margin, New Zealand. Tectonics 12, pp. 1365–1379.
9. Bettis III, E.A., Muhs, D.R., Roberts, H.M., Wintle, A.G. 2003. Last glacial loess in the conterminous USA. Quaternary Science Reviews 22, pp. 1907–1946.
10. Bokhorst, M.P., Beets, C.J., Marković, S.B., Gerasimenko, N.P., Matviishina, Z.N., Frechen, M. 2009. Pedo-chemical climate proxies in Late Pleistocene Serbian-Ukrainian loess sequences. Quaternary International 198, pp. 113-123.
11. Bokhorst, M.P., Vandenberghe, J. 2009. Validation of wiggle matching using multi-proxy approach and its palaeoclimatic significance. Journal of Quaternary Science 24, pp. 937-947.
12. Bronger, A. 2003. Correlation of loess–paleosol sequences in East and Central Asia with SE Central Europe—towards a continental Quaternary pedostratigraphy and paleoclimatic history. Quaternary International 106–107, pp. 11–31.
13. Buggle, B., Glaser, B., Zöller, L., Hambach, U., Marković, S.B., Glaser, I., Gerasimenko, N. 2008. Geochemical characterization and origin of Southeastern and Eastern European loesses (Serbia, Romania, Ukraine). Quaternary Science Reviews 27, pp. 1058–1075.
14. Buggle, B., Hambach, U., Glaser, B., Gerasimenko, N., Markovic, S., Glaser, I., Zöller, L. 2009. Stratigraphy, and spatial and temporal paleoclimatic trends in Southeastern/Eastern European loess-paleosol sequences. Quaternary International 196, pp. 86-106.

15. Buggle, B., Hambach, U., Kehl, M., Marković, S.B., Zöller, L., Glaser, B. 2013. The progressive evolution of a continental climate in southeast-central European lowlands during the Middle Pleistocene recorded in loess paleosol sequences. Geology 41, pp. 771–774.

16. Buggle, B., Hambach, U., Müller, K., Zöller, L., Marković, S.B., Glaser, B. 2014. Iron mineralogical proxies and Quaternary climate change in SE-European loess-paleosol sequences. Catena 117, pp. 4–22.

17. Burow, C. 2020. calc_CentralDose(): Apply the central age model (CAM) after Galbraith et al. (1999) to a given De distribution. Function version 1.4.0. In: Kreutzer, S., Burow, C., Dietze, M., Fuchs, M.C., Schmidt, C., Fischer, M., Friedrich, J. 2020. Luminescence: Comprehensive Luminescence Dating Data Analysis. R package version 0.9.7. https://CRAN.R-project.org/package=Luminescence.

18. Busacca, A.J., Begét, J.E., Markewich, H.W., Muhs, D.R., Lancaster, N., Sweeney, M.R. 2004. Eolian sediments. In: Gillespie, A.R., Porter, S.C., Atwater, B.F. (Eds.), The Quaternary period in the United States. Elsevier, Amsterdam, Netherlands, pp. 275–309.

19. Buylaert, J.P, Murray, A.S., Vandenberghe, D., Vriend, M., De Corte, F., Van den haute, P. 2008. Optical dating of Chinese loess using sand-sized quartz: Establishing a time frame for Late Pleistocene climate changes in the western part of the Chinese Loess Plateau. Quaternary Geochronology 5, pp. 143–148.

20. Buylaert, J.P., Vandenberghe, D., Murray, A.S., Huot, S., De Corte, F., Van den Haute, P. 2007. Luminescence dating of old (>70 ka) Chinese loess: A comparison of single aliquot OSL and IRSL techniques. Quaternary Geochronology 10, pp. 75–80.

21. Chapot, M.S., Roberts, H.M., Duller, G.A.T., Lai, Z.P. 2012. A comparison of natural-and laboratory-generated dose response curves for quartz optically stimulated luminescence signals from Chinese Loess. Radiation Measurements 47, pp. 1045-1052.

22. Conard, N.J., Bolus, M. 2003. Radiocarbon dating the appearance of modern humans and timing of cultural innovations in Europe: new results and new challenges. Journal of Human Evolution 44, pp. 331–371.

23. Conea A. 1969. Profils de lœss en Roumanie. In: Fink, J. (Ed.), La stratigraphie des lœss d'Europe. Supplément du Bulletin de l'Association Française pour l'Etude du Quaternaire, INQUA, pp. 127-134.

24. Conea, A. 1970. Formatiuni Cuaternare în Dobrogea (Loessuri si Paleosoluri) (Quaternary Units in Dobrogea), Editura Academiei RSR, Bucuresti, Romania, pp. 234.

25. Constantin, D., Begy, R., Vasiliniuc, S., Panaiotu, C., Necula, C., Codrea, V., Timar-Gabor, A. 2014. High-resolution OSL dating of the Costinești section (Dobrogea, SE Romania) using fine and coarse quartz. Quaternary International 334-335, pp. 20-29.

26. Constantin, D., Camenita, A., Panaiotu, C., Necula, C., Codrea, V., Timar-Gabor, A. 2015a. Fine and coarse-quartz SAR-OSL dating of Last Glacial loess in Southern Romania. Quaternary International 357, pp. 33-43.

27. Constantin, D., Jain, M., Murray, A.S., Buylaert, J.-P., Timar-Gabor, A. 2015b. Quartz luminescence response to a mixed alpha - beta field: Investigations on Romanian loess. Radiation Measurements 81, pp. 110-115.

28. Constantin, D., Timar-Gabor, A., Veres, D., Begy, R., Cosma, C. 2012. SAR-OSL dating of different grain-sized quartz from a sedimentary section in southern Romania interbedding the Campanian Ignimbrite/Y5 ash layer. Quaternary Geochronology 10, pp. 81-86.

29. Constantin, D., Veres, D., Panaiotu, C., Anechitei-Deacu, V., Groza, S.M., Begy, R., Kelemen, S., Buylaert, J.P., Hambach, U., Marković, S.B. 2019. Luminescence age constraints on the Pleistocene-Holocene transition recorded in loess sequences across SE Europe. Quaternary Geochronology 49, pp. 71–77.

30. Cunningham, A.C., Murray, A.S., Armitage, S.J., Autzen, M. 2018. High-precision natural dose rate estimates through beta counting. Radiation Measurement 120, pp. 209-214.

31. Dimofte, D., 2012. Schimbări climatice cuaternare înregistrate în depozite sedimentare deduse prin analize mineralogice, granulometrice, geochimice şi magnetice pe secţiuni de loess-paleosol din România Climatic fluctuation recorded by loess-paleosol deposits from Romania using mineralogical, granulometric, geochemical and magnetic data. PhD thesis. University of Bucharest, pp. 165 (in Romanian).

32. Dodonov, A. E., Zhou, L.P., Markova, A.K., Tchepalyga, A.L., Trubikin, V. M., Aleksandrowski, A.L., Simakova, A.N. 2006. Middle-Upper Pleistocene bio-climatic and magnetic records of the Northern Black Sea Coastal Area. Quaternary International 149, pp. 44-54.

33. Dong, G., Yang, Y., Zhao, Y., Zhou, A., Zhang, X., Li, X., Chen, F. 2012. Human settlement and human-environment interactions during the historical period in Zhuanglang County, western Loess Plateau. Quaternary International 281, pp. 78–83.

34. Duller, G.A.T. 2004. Luminescence dating of Quaternary sediments: recent advances. Journal of Quaternary Science 19, pp. 183-192.

35. Duller, G.A.T., Bøtter-Jensen, L., Murray, A.S. 2000. Optical dating of single sand-sized grains of quartz: sources of variability. - Radiation Measurements 32, pp. 453-457.

36. Eden, D.N. Hammond, A.P. 2003. Dust accumulation in the New Zealand region since the last glacial maximum. Quaternary Science Reviews 22, pp. 2037–2052.

37. Einwögerer, T., Friesinger, H., Händel, M., Neugebauer-Maresch, C., Simon, U. 2006. Upper Palaeolithic infant burials. Decorations on the bodies of newborns indicate that they were probably important in their community. Nature 444, pp. 285.

38. Einwögerer, T., Händel, M., Neugebauer-Maresch, C., Simon, U., Steier, P., Teschler-Nicola, M., Wild, E.M. 2009. ^{14}C dating of the Upper Paleolithic site at Krems-Wachtberg, Austria. Radiocarbon 51, pp. 847-855.

39. Einwögerer, T., Händel, M., Simon, U., Masur, A., Neugebauer-Maresch, C. 2014. Upper Palaeolithic occupation in the Wachtberg area of Krems: The evidence of surveys, sections and core samples, Quaternary International 351, pp. 50-66.

40. Forman, S.L., 1991. Late Pleistocene chronology of loess deposition near Luochuan, China. Quaternary Research 36, pp. 19-28.

41. Fu, X., Li, B., Li, S.H. 2012. Testing a multi-step post-IR IRSL dating method using polymineral fine grains from Chinese loess. Quaternary Geochronology 10, pp. 8-15.

42. Galbraith, R.F., Roberts, R.G., Laslett, G.M., Yoshida, H., Olley, J.M. 1999. Optical dating of single grains of quartz from Jinmium rock shelter, northern Australia. Part I: experimental design and statistical models. Archaeometry 41, pp. 339-364.

43. Gallet, S., Jahn, B., Torii, M. 1996. Geochemical characterization of the Luochuan loess-paleosol sequence, China, and paleoclimatic implications. Chemical Geology 133, pp. 67-88.

44. Groza, S.M., Hambach, U., Veres, D., Vulpoi, A., Händel, M., Einwögerer, T., Simon, U., Neugebauer-Maresch, C., Timar-Gabor, A. 2019. Optically stimulated luminescence ages for the Upper Palaeolithic site Krems-Wachtberg, Austria. Quaternary Geochronology 49, pp. 242-248.

45. Groza-Săcaciu, S.M., Panaiotu, C., Timar-Gabor, A. 2020. Single aliquot regeneration (SAR) optically stimulated luminescence dating protocols using different grains-sizes of quartz: Revisiting the chronology of Mircea Vodă loess-paleosol master section (Romania). Methods and Protocols 3, 19.

46. Guérin, G., Mercier, N., Adamiec, G. 2011. Dose-rate conversion factors: Update. Ancient TL 29, pp. 5-8.

47. Haesaerts, P. 1990. Stratigraphy of Grubgraben Loess Sequence. In: Montet-White, A. (Ed.) The Epigravettian Site of Grubgraben, Lower Austria: The 1986 and 1987 Excavations. ERAUL 40, Liège, pp. 15-35.

48. Haesaerts, P., Damblon, F. 2016. The Late Palaeolithic Site of Kammern-Grubgraben (Lower Austria). Additional Data on Loess Stratigraphy and Palaeoenvironment. Archaeologia Austriaca 100, pp. 255-269.

49. Hambach, U. 2010. Palaeoclimatic and stratigraphic implications of high resolution magnetic susceptibility logging of Würmian loess at the Krems–Wachtberg Upper-Palaeolithic site. In: Neugebauer-Maresch, C., Owen, L.R. (Eds.), New aspects of the Central and Eastern European Upper Palaeolithic — methods, chronology, technology and subsistence. Proceedings of the Prehistoric Commission of the Austrian Academy of Sciences, Vienna, Austria, pp. 295–304.

50. Hambach, U., Zeeden, C., Hark, M., Zöller, L. 2008. Magnetic dating of an Upper Palaeolithic cultural layer bearing loess from the Krems-Wachtberg site (lower Austria), Abhandlungen der Geologischen Bundesanstalt 62, pp. 153-157.

51. Händel, M., Einwögerer, T., Simon, U. 2008. Krems-Wachtberg - a Gravettian settlement site in the Middle Danube Region. Wissenschaftliche Mitteilungen des Niederösterreichischen Landesmuseum 19, pp. 91-108.

52. Händel, M., Einwögerer, T., Simon, U., Neugebauer-Maresch, C. 2014. Krems-Wachtberg excavations 2005–12: main profiles, sampling, stratigraphy, and site formation. Quaternary International 351, pp. 38-49.

53. Händel, M., Simon, U., Einwögerer, T., and Neugebauer-Maresch, C. 2009. Loess deposits and the conservation of the archaeological record – the Krems-Wachtberg example. Quaternary International 198, pp. 46–50.

54. Händel, M., Simon, U., Maier, A., Brandl, M., Groza-Săcaciu, S.M., Timar-Gabor, A., Einwögerer, T. 2020. Kammern-Grubgraben revisited - First results from renewed investigations at a well-known LGM site in East Austria. Quaternary International *in press*.

55. Heller, F., Liu, T.S. 1984. Magnetism of Chinese loess deposits. Geophysical Journal International 77, pp. 125–141.

56. Huntley, D.J., Godfrey-Smith, D.I., Thewalt, M.L.W. 1985. Optical dating of sediments. Nature 313, pp. 105–107.

57. Iovita, R., Doboş, A., Fitzsimmons, K. E., Probst, M., Hambach, U., Robu, M., Vlaicu, M., Petculescu, A. 2014. Geoarchaeological prospection in the loess steppe: Preliminary results from the Lower Danube Survey for Paleolithic Sites (LoDanS). Quaternary International 351, pp. 98–114.

58. Jacobs, P.M., Mason, J.A. 2007. Late Quaternary climate change, loess sedimentation, and soil profile development in the central Great Plains: A pedosedimentary model. Geological Society of America Bulletin 119, pp. 462-475.

59. Kind, C.-J. 2000. Die jungpleistozänen Rinnenfüllungen von Nußloch (Rhein-Neckar-Kreis). Archäologische Ausgrabungen Baden-Württemberg 1999, 17-19.

60. Kukla, G., An, Z. 1989. Loess stratigraphy in central China. Palaeogeography, Palaeoclimatology, Palaeoecology 72, pp. 203–225.

61. Kukla, G., Heller, F., Liu, X.M., Xu, T.C., Liu, T.S., An, Z.S. 1988. Pleistocene climates in China dated by magnetic susceptibility. Geology 16, pp. 811–814.

62. Lai, Z., Fan, A. 2014. Examining quartz OSL age underestimation for loess samples from Luochuan in the Chinese Loess Plateau. Geochronometria 41, pp. 57-64.

63. Lai, Z.P. 2010. Chronology and the upper dating limit for loess samples from Luochuan section in the Chinese Loess Plateau using quartz OSL SAR protocol. Journal of Asian Earth Sciences 37, pp. 176-185.

64. Lai, Z.-P., Wintle, A.G. 2006. Locating the boundary between the Pleistocene and the Holocene in Chinese loess using luminescence. The Holocene 16, pp. 893-899.

65. Li, B., Li, S.-H. 2012. Luminescence dating of Chinese loess beyond 130 ka using the non-fading signal from K-feldspar. Quaternary Geochronology 10, pp. 24-31.

66. Li, Y., Shi, W., Aydin, A., Beroya-Eitner, M.A., Gao, G. 2020. Loess genesis and worldwide distribution. Earth-Science Reviews 201, pp. 1029-1047.

67. Lisiecki, L.E., Raymo, M.E. 2005. A Pliocene-Pleistocene stack of 57 globally distributed benthic δ18O records. Paleoceanography 20, PA1003.

68. Liu, T.S. (Ed.) 1985. Loess and the environment. China Ocean Press, Beijing, China, pp. 251.

69. Lomax, J., Fuchs, M., Preusser, F., Fiebig, M., 2014. Luminescence loess chronostratigraphy of the Upper Palaeolithic site Krems-Wachtberg, Austria, Quaternary International 351, pp. 88-97.

70. Lu, H., Stevens, T., Yi, S., Sun, X. 2006. An erosional hiatus in Chinese loess sequences revealed by closely spaced optical dating, Chinese Science Bulletin 18, pp. 2253-2259.

71. Lu, H., Yi, S., Liu, Z., Mason, J.A., Jiang, D., Cheng, J., Stevens, T., Xu, Z., Zhang, E., Jin, L., Zhang, Z., Guo, Z., Wang, Y., Otto-Bliesner, B. 2013. Variation of East Asian monsoon precipitation during the past 21 k.y. and potential CO_2 forcing, Geology 41, pp. 1023-1026.

72. Lu, Y.C. Wang, X.L., Wintle, A.G. 2007. A new OSL chronology for dust accumulation in the last 130,000 yr for the Chinese Loess Plateau. Quaternary Research 67, pp. 152-160.

73. Marković, S.B., Bokhorst, M., Vandenberghe, J., McCoy, W.D., Oches, E.A., Hambach, U., Gaudenyi, T., Jovanović, M., Zöller, L., Stevens, T., Machalett, B. 2008. Late Pleistocene loess–paleosol sequences in the Vojvodina region, North Serbia. Journal of Quaternary Science 23, pp. 73–84.

74. Marković, S.B., Stevens, T., Kukla, G.J., Hambach, U., Fitzsimmons, K.E., Gibbard, P., Buggle, B., Zech, M., Guoi, Z., Haoi, Q., Wui, H., O'Hara Dhand, K., Smalley, I.J., Újvári, G., Sümegi, P., Timar-Gabor, A., Veres, D., Sirocko, F., Vasiljević, D.A., Jary, Z., Svensson, A., Jović, V., Lehmkuhl, F., Kovácsu, J., Svirčeva, Z. 2015. Danube loess stratigraphy - towards a pan-European loess stratigraphic model. Earth Science Reviews 148, pp. 228–258.

75. Mejdahl, V. 1979. Thermoluminescence dating: Beta-dose attenuation in quartz grains. Archaeometry 21, pp. 61–72.

76. Mellars, P. 2011. Palaeoanthropology: The earliest modern humans in Europe. Nature 479, pp. 483–485.

77. Milankovitch, M.M. 1949. Kanon der Erdbestrahlung und seine Anwendung auf das Eiszeitenproblem. Royal Serbian Sciences, Spec. pub. 132, Section of Mathematical and Natural Sciences, 33, Belgrade, pp. 633 (Canon of Insolation and the Ice Age Problem, English translation by Israel Program for Scientific Translation and published for the U.S. Department of Commerce and the National Science Foundation, Washington D.C., 1969).

78. Muhs, D.R. 2007. Loess deposits, origins, and properties. In: Elias, S. (Ed.), The encyclopedia of Quaternary sciences. Elsevier, Amsterdam, Netherlands, pp. 1405–1418.

79. Muhs, D.R. 2013. The geologic records of dust in the Quaternary. Aeolian Research 9, pp. 3–48.

80. Muhs, D.R., Bettis. E.A. III. 2003. Quaternary loess-paleosol sequences as examples of climate -driven sedimentary extremes. Special Paper of the Geological Society of America 370, pp. 53–74.

81. Muhs, D.R., Cattle, S.R., Crouvi, O., Rousseau, D.D., Sun, J.M., Zárate, M.A. 2014. Loess records. In: Knippertz, P., Stuut, J.W. (Eds.), Mineral Dust: A Key Player in the Earth System. Springer Verlag, Berlin, Germany, pp. 411–441.

82. Murray, A.S., Olley, J.M. 2002. Precision and accuracy in the optically stimulated luminescence dating of sedimentary quartz: a status review. Geochronometria 21, pp. 1-16.

83. Murray, A.S., Svendsen, J.I., Mangerund, J.I., Astakhov, V.I. 2007. Testing the accuracy of quartz OSL dating using a known-age Eemian site on the river Sula, northern Russia. Quaternary Geochronology 2, pp. 102–109.

84. Murray, A.S., Wintle, A.G. 2000. Luminescence dating of quartz using an improved single-aliquot regenerative-dose protocol. Radiation Measurements. 32, pp. 57–73.

85. Murray, A.S., Wintle, A.G. 2003. The single aliquot regenerative dose protocol: potential for improvements in reliability. Radiation Measurements 37, pp. 377-381.

86. Nawrocki, J., Gozhik, P., Łanczont, M., Pańczyk, M., Komar, M., Bogucki, A., Williams, I.S., Czupyt, Z. 2018. Palaeowind directions and sources of detrital material archived in the Roxolany loess section (southern Ukraine). Palaeogeography, Palaeoclimatology, Palaeoecology 496, pp. 121-135.

87. Necula, C., Panaiotu, C. 2012. Rock magnetic properties of a loess-paleosols complex from Mircea Vodă (Romania). Romanian Reports in Physics 64, pp. 516–527.

88. Necula, C., Panaiotu, C., Heslop, D., Dimofte, D. 2013. Climatic control of magnetic granulometry in the Mircea Vodă loess/paleosol sequence (Dobrogea, Romania). Quaternary International 293, pp. 5–14.

89. Nugteren, G., Vandenberghe, J., van Huissteden, J.K., Zhisheng, A. 2004. A Quaternary climate record based on grain size analysis from the Luochuan loess section on the Central Loess Plateau, China. Global and Planetary Change 41, pp. 167-183.

90. Panaiotu, C.G., Panaiotu, E.C., Grama, A., Necula, C. 2001. Paleoclimatic Record from a Loess-Paleosol Profile in Southeastern Romania. Physics and Chemistry of the Earth A 26, pp. 893–989.

91. Péwé, T.L. 1975. Quaternary geology of Alaska. US Geological Survey Professional Paper 835, pp. 1–145.

92. Prescott, J.R., Hutton, J.T. 1994. Cosmic ray contributions to dose rates for Luminescence and ESR Dating: large depths and long-term variations. Radiation Measurements 23, pp. 497-500.

93. Preusser, F., Chithambo, M., L., Götte, T., Martini, M., Ramseyer, K., Sendezera, E., J., Susino, G., J., Wintle, A., G., 2009. Quartz as a natural luminescence dosimeter. Earth-Science Reviews, 97, pp. 184-214.

94. Pye, K. 1987. Aeolian Dust and Dust Deposits. Academic Press: San Diego, CA, USA, pp. 334.

95. Pye, K. 1995. The nature, origin and accumulation of loess. Quaternary Science Reviews 14, pp. 653–657.

96. Rees-Jones, J. 1995. Optical dating of young sediments using fine-grain quartz. Ancient TL 13, pp. 9–14.

97. Rees-Jones, J., Tite, M.S. 1997. Optical dating results for British archeological sediments. Archaeometry 39, pp. 177-187.

98. Roberts, H.M. 2008. The development and application of luminescence dating to loess deposits: a perspective on the past, present and future. Boreas 37, pp. 483–507.

99. Schaetzl, R.J., Anderson, S. (Eds.), 2005. Soils: Genesis and Geomorphology. Cambridge University Press, New York, USA, pp. 817.

100. Smalley, I.J. 1968. The loess deposits and Neolithic culture of northern China. Man 3, pp. 224–241.

101. Smith, B.W., Rhodes, E.J. 1994. Charge movements in quartz and their relevance to optical dating. Radiation Measurements, 23, pp. 329-333.

102. Stern, J.V., Lisiecki, L.E. 2014. Termination 1 timing in radiocarbon-dated regional benthic $\delta^{18}O$ stacks. Paleoceanography 29, pp. 1127–1142.

103. Stevens T., Buylaert, J.P., Thiel, C., Újvári, G.,Yi, S., Murray, A.S., Frechen M., Lu, H. 2018. Ice-volume-forced erosion of the Chinese Loess Plateau global Quaternary stratotype site. Nature Communications 9, pp. 983.

104. Stevens, T., Armitage, S.J., Lu, H., Thomas D.S.G. 2007a. Examining the potential of high sampling resolution OSL dating of Chinese loess, Quaternary Geochronology 2, pp. 15-22.

105. Stevens, T., Armitage, S.J., Lu, H.Y., Thomas, D.S.G. 2006. Sedimentation and diagenesis of Chinese loess: implications for the preservation of continuous, high-resolution climate records. Geology 34, pp. 849-852.

106. Stevens, T., Thomas, D.S.G., Armitage, S.J., Lunn, H.R., Lu, H. 2007b. Reinterpreting climate proxy records from late Quaternary Chinese loess: A detailed OSL investigation. Earth-Science Reviews 80, pp. 111-136.

107. Terhorst, B., Sedov, S., Sprafke, T., Peticzka, R., Meyer-Heintze, S., Kühn, P., Solleiro Rebolledo, E. 2015. Austrian MIS 3/2 loess-palaeosol records – key sites along a west-east transect. Palaeogeography. Palaeoclimatology. Palaeoecology. 418, pp. 43–56.

108. Thomsen, K.J., Bøtter-Jensen, L., Denby, P.M., Moska, P., Murray, A.S. 2006. Developments in luminescence measurement techniques. Radiation Measurements 41, pp. 768–773.

109. Thomsen, K.J., Bøtter-Jensen, L., Jain, M., Denby, P.M., Murray, A.S. 2008. Recent instrumental developments for trapped electron dosimetry. Radiation Measurements 43, pp. 414–521.

110. Timar, A., Vandenberghe, D., Panaiotu, E.C., Panaiotu, C.G., Necula, C., Cosma, C., van den haute, P. 2010. Optical dating of Romanian loess using fine-grained quartz. Quaternary Geochronology 5, pp. 143–148.

111. Timar-Gabor, A., Buylaert, J.-P., Guralnik, B., Trandafir-Antohi, O., Constantin, D., Anechitei-Deacu, V., Jain, M., Murray, A.S., Porat, N., Hao, Q., Wintle, A.G. 2017. On the

importance of grain size in luminescence dating using quartz. Radiation Measurements 106, pp. 464-471.

112. Timar-Gabor, A., Constantin, D., Buylaert, J.P., Jain, M., Murray, A.S., Wintle, A.G. 2015b. Fundamental investigations of natural and laboratory generated SAR dose response curves for quartz OSL in the high dose range. Radiation Measurements 81, pp. 150-156.

113. Timar-Gabor, A., Constantin, D., Marković, S.B., Jain, M. 2015a. Extending the area of investigation of fine versus coarse quartz optical ages from the Lower Danube to the Carpathian Basin. Quaternary International 388, pp. 168-176.

114. Timar-Gabor, A., Vandenberghe, D.A.G., Vasiliniuc, S., Panaiotu, C.E., Panaiotu, C.G., Dimofte, D., Cosma, C. 2011. Optical dating of Romanian loess: A comparison between silt-sized and sand-sized quartz. Quaternary International 240, pp. 62–70.

115. Timar-Gabor, A., Vasiliniuc, S., Vandenberghe, D.A.G., Cosma, C., Wintle, A.G. 2012. Investigations into the reliability of SAR-OSL equivalent doses obtained for quartz samples displaying dose response curves with more than one component. Radiation Measurements 47, pp. 740–745.

116. Timar-Gabor, A., Wintle, A.G. 2013. On natural and laboratory generated dose response curves for quartz of different grain sizes from Romanian loess. Quaternary Geochronology 18, pp. 34-40.

117. Trandafir, O., Timar-Gabor, A., Schmidt, C., Veres, D., Anghelinu, M., Hambach, U., Simon, S. 2015. OSL dating of fine and coarse quartz from a Palaeolithic sequence on the Bistrita Valley (northeastern Romania). Quaternary Geochronology 30, pp. 487-492.

118. Vandenberghe, D., De Corte, F., Buylaert, J.-P., Kučera, J., Van den haute, P. 2008. On the internal radioactivity of quartz. Radiation Measurements 43, pp. 771–775.

119. Vasiliniuc, Ș., Vandenberghe, D.A.G., Timar-Gabor, A., Cosma, C., van den Haute, P. 2013a. Combined IRSL and post-IR OSL dating of Romanian loess using single aliquots of polymineral fine grains. Quaternary International 293, pp. 15–21.

120. Vasiliniuc, Ș., Vandenberghe, D.A.G., Timar-Gabor, A., Panaiotu, C., Cosma, C., van den Haute, P. 2012. Testing the potential of elevated temperature post-IR IRSL signals for dating Romanian loess. Quaternary Geochronology 10, pp. 75–80.

121. Vasiliniuc, S., Vandenberghe, D.A.G., Timar-Gabor, A., Van Den haute, P. 2013b. Conventional IRSL dating of Romanian loess using single aliquots of polymineral fine grains. Radiation Measurements 48, pp. 60–67.

122. Verosub, K.L., Fine, P., Singer, M.J., TenPas, J. 1993. Pedogenesis and paleoclimate: interpretation of the magnetic susceptibility record of Chinese loess-paleosol sequences. Geology 21, pp. 1011–1014.

123. Wintle, A.G., 2008. Luminescence dating: where it has been and where it is going. Boreas 37, pp. 471–482.

124. Wintle, A.G., Adamiec, G. 2017. Optically stimulated luminescence signals from quartz: A review. Radiation Measurements 98, pp. 10-33.

125. Yang, J.-D., Chen, J., Tao, X.-C., Li, C.-L., Ji, J.-F., Chen, Y. 2001. Sr isotope ratios of acid-leached loess residues from Luochuan, China: A tracer of continental weathering intensity over the past 2.5 Ma. Geochemical Journal 35, pp. 403-412.

126. Zárate, M.A. 2003. Loess of southern South America. Quaternary Science Reviews 22, pp. 1987–2006.

127. Zárate, M.A. 2017. Eolian Settings: Loess. In: Gilbert, A.S. (Ed.), Encyclopedia of Geoarchaeology. Encyclopedia of Earth Sciences Series. Springer, Dordrecht, Netherlands, pp. 233-238.

128. Zech, M., Kreutzer, S., Zech, R., Goslar, T., Meszner, S., McIntyre, C., Häggi, C., Eglinton, T., Faust, D. and Fuchs, M. 2017. Comparative ^{14}C and OSL dating of loess-paleosol sequences to evaluate post-depositional contamination of n-alkane biomarkers. Quaternary Research, 87, pp. 180-189.

129. Zeeden, C., Hambach, U., Händel, M. 2015. Loess magnetic fabric of the Krems-Wachtberg archaeological site. Quaternary International 372, pp. 188-194.

130. Zeeden, C., Hambach, U., Händel, M. 2015. Loess magnetic fabric of the Krems-Wachtberg archaeological site. Quaternary International 372, pp. 188-194.

131. Zhang, H.C., Yang, M.S., Zhang, Q.X., Lei, G.L., Chang, F.Q., Pu, Y., Fan, H.F. 2008. Molecular fossil and paleovegetation records of paleosol S4 and adjacent loess layers in the Luochuan loess section, NW China. Science in China Series D: Earth Sciences 51, pp. 321-330.

132. Zhisheng, A, Kukla, G., Tungsheng, L. 1989. Loess stratigraphy in Luochuan of China. Quaternary Sciences 2, pp. 155-168.

133. Zöller, L., Richter, D., Blanchard, H., Einwögerer, T., Händel, M., Neugebauer-Maresch, C. 2014. Our oldest children: Age constraints for the Krems-Wachtberg site obtained from various thermoluminescence dating approaches. Quaternary International 351, pp. 83-87.